$(F_8TPP)Fe^{II}/O_2$ Reactivity Studies {F_8TPP = Tetrakis(2,6-difluorophenyl)porphyrinate(2−)}: Spectroscopic (UV−Visible and NMR) and Kinetic Study of Solvent-Dependent (Fe/O_2 = 1:1 or 2:1) Reversible O_2-Reduction and Ferryl Formation

Reza A. Ghiladi,[†] Ryan M. Kretzer,[†] Ilia Guzei,[‡] Arnold L. Rheingold,[‡] Yorck-Michael Neuhold,[§] Karen R. Hatwell,[§] Andreas D. Zuberbühler,[§] and Kenneth D. Karlin*,[†]

Department of Chemistry, The Johns Hopkins University, Charles and 34th Streets, Baltimore, Maryland 21218, Department of Chemistry, University of Delaware, Newark, Delaware 19716, and Institute für Anorganische Chemie, University of Basel, CH-4056 Basel, Switzerland

Received June 4, 2001

In this report, we describe in detail the O_2-binding chemistry of the metalloporphyrin $(F_8TPP)Fe^{II}$ (**1**). This complex was synthesized from aqueous dithionite reduction of $(F_8TPP)Fe^{III}$-Cl (X-ray structure reported: $C_{55}H_{36}ClF_8FeN_4O$; a = 13.6517(2) Å, b = 13.6475(2) Å, c = 26.3896(4), α = 90°, β = 89.9776(4)°, γ = 90°; monoclinic, $P2(1)/c$, Z = 4). Complex **1** crystallizes from toluene/heptane solvent system as a bis(toluene) solvate, $(F_8TPP)Fe^{II}\cdot(C_7H_8)_2$, with ferrous ion in the porphyrin plane ($C_{58}H_{36}F_8FeN_4$; a = 20.9177(2) Å, b = 11.7738(2) Å, c = 19.3875(2), α = 90°, β = 108.6999(6)°, γ = 90°; monoclinic, $C2/c$, Z = 4; Fe−N_4(av) = 2.002 Å; N−Fe−N (all) = 90.0°). Close metal−arene contacts are also observed at 3.11−3.15 Å. Upon oxygenation of **1** at 193 K in coordinating solvents, UV−visible and ^2H and ^{19}F NMR spectroscopies revealed the presence of a reversibly formed dioxygen adduct, formulated as the heme-superoxo complex $(S)(F_8TPP)Fe^{III}$-(O_2^-) (**2**) (S = solvent) [(i) tetrahydrofuran (THF) solvent: UV−visible, 416 (Soret), 536 nm; ^2H NMR: $\delta_{pyrrole}$ 8.9 ppm; (ii) EtCN solvent: UV−visible, 414 (Soret), 536 nm; (iii) acetone solvent: UV−visible, 416 (Soret), 537 nm; ^2H NMR: $\delta_{pyrrole}$ 8.9 ppm]. Dioxygen-uptake manometry (THF, 193 K) revealed an O_2:**1** oxygenation stoichiometry of 1.02:1, consistent with the heme-superoxo formulation of **2**. Stopped-flow UV−visible spectrophotometry studies of the $(F_8TPP)Fe^{II}$ (**1**)/O_2 reaction in EtCN and THF solvents were able to provide kinetic and thermodynamic insight into the reversible formation of **2** [(i) EtCN: $\Delta H^\circ = -40 \pm 5$ kJ/mol; $\Delta S^\circ = -105 \pm 23$ J/(K mol); $k_1 = (5.57 \pm 0.04) \times 10^3$ M^{-1} s^{-1} (183 K); $\Delta H^\ddagger = 38.6 \pm 0.2$ kJ/mol; $\Delta S^\ddagger = 42 \pm 1$ J/(K mol); (ii) THF: $\Delta H^\circ = -37.5 \pm 0.4$ kJ/mol; $\Delta S^\circ = -109 \pm 2$ J/(K mol)}. The $(F_8TPP)Fe^{II}$ (**1**)/O_2 reaction was also examined at reduced temperatures in noncoordinating solvents (toluene, CH_2Cl_2), where UV−visible and ^2H and ^{19}F NMR spectroscopies also revealed the presence of a reversibly formed adduct, formulated as the peroxo-bridged dinuclear complex $[(F_8TPP)Fe^{III}]_2$-(O_2^{2-}) (**3**) [CH_2Cl_2: UV−visible, 414 (Soret), 535 nm; ^2H NMR, $\delta_{pyrrole}$ 17.5 ppm]. Dioxygen-uptake spectrophotometric titrations revealed a stoichiometry of 2 $(F_8TPP)Fe^{II}$ (**1**) per O_2 upon full formation of **3**. Addition of a nitrogenous base, 4-(dimethylamino)pyridine, to a cold solution of **3** in dichloromethane gave rapid formation of the iron(IV)-oxo ferryl species $(DMAP)(F_8TPP)Fe^{IV}$=O (**4**), based upon UV−visible [417 (Soret), 541 nm] and ^2H NMR ($\delta_{pyrrole}$ = 3.5 ppm) spectroscopic characterization. These detailed investigations into the O_2-adducts and "ferryl" species formed from $(F_8TPP)Fe^{II}$ (**1**) may be potentially important for a full understanding of our ongoing heme-copper oxidase model studies, which employ **1** or similar "tethered" (i.e., covalently attached Cu-chelate) porphyrin analogues in heme/Cu heterobinuclear systems.

Introduction

Given the importance and essential nature of dioxygen transport and storage by hemoglobin and myoglobin, investigations of O_2-binding and reduction by synthetic porphyrinate−iron(II) complexes with O_2 have unceasingly and deservedly attracted considerable interest.[1−7] A new resurgence into heme-O_2 chemistry has also been ignited by the recent studies on heme-protein sensors[8,9] of small molecule gases, such as O_2 (e.g., FixL),[10,11] CO (e.g., CooA),[12−14] and NO (e.g., guanylate

* Corresponding author.
† The Johns Hopkins University.
‡ University of Delaware.
§ University of Basel.

(1) Momenteau, M.; Reed, C. A. *Chem. Rev.* **1994**, *94*, 659−698.
(2) Traylor, T. G.; Traylor, P. S. In *Active Oxygen: Active Oxygen in Biochemistry*; Valentine, J. S., Foote, C. S., Greenberg, A., Liebman, J. F., Eds.; Chapman & Hall: New York, 1995; pp 84−187.
(3) Bakac, A. *Prog. Inorg. Chem.* **1995**, *43*, 267−351.
(4) Collman, J. P.; Halbert, T. R.; Suslick, K. S. In *Metal Ion Activation of Dioxygen*; Spiro, T. G., Ed.; John Wiley & Sons: New York, 1980; pp 1−72.
(5) Collman, J. P. *Inorg. Chem.* **1997**, *36*, 5145−5155.
(6) Collman, J. P.; Eberspacher, T.; Fu, L.; Herrmann, P. C. *J. Mol. Catal. A: Chem.* **1997**, *117*, 9−20.
(7) Collman, J. P.; Fu, L. *Acc. Chem. Res.* **1999**, *32*, 455−463.
(8) Rodgers, K. R. *Curr. Opin. Chem. Biol.* **1999**, *3*, 158−167.
(9) Chan, M. K. *J. Porphyrins Phthalocyanines* **2000**, *4*, 358−361.

10.1021/ic0105866 CCC: $20.00
Published on Web 10/10/2001

cyclase).[15,16] Such inquiries also bear upon dioxygen activation chemistry,[17−20] such as that occurring in the cytochrome P-450 monooxygenase enzymes.[17,18,21,22] More recent biomimetic efforts into non-heme Fe−O_2[23,24] or Cu−O_2[25−29] chemical systems have focused on other classes of dioxygen-transport metalloproteins, such as in model compounds for hemerythrin, the non-heme diiron O_2-carrier of marine worms,[30−32] and hemocyanin, a copper-containing arthropodal and molluscan O_2-carrier protein.[25,33,34]

Our own interests in this area come from a combination of heme and copper dioxygen chemistry, as is important at the active site of heme-copper oxidase proton pumps such as cytochrome *c* oxidase. Recent biochemical and notable protein X-ray structural advances[35−40] reveal that O_2-binding and reduction occurs at a heterobinuclear active site consisting of a high-spin heme group (with proximal histidine), located ∼4.5 Å from Cu_B, which possesses three histidine nitrogen ligands. While an initial O_2 interaction with Cu_B has been postulated,[41,42] the latest emerging picture is that the metal-O_2 chemistry is dominated by the heme, with Cu_B being critical for electron-transfer and proton-translocation chemistry.[37,39,43−46] Thus, an emphasis of our research program is focused upon elucidating the fundamental aspects of O_2-interactions with heme-copper centers, by looking at how a copper ion influences (**P**)Fe^{II}/O_2 chemistry (**P** = porphyrinate) and how hemes impact already known copper(I)−dioxygen reactivity patterns.

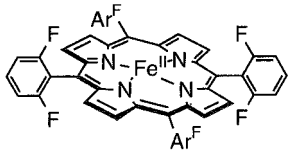

$(F_8TPP)Fe^{II}$ (**1**)

To these ends, we have been studying the dioxygen reactivity of 1:1 mixtures (i.e., "untethered" systems) of the porphyrinate−iron(II) complex $(F_8TPP)Fe^{II}$ (**1**) (see diagram; Ar^F = 2,6-difluorophenyl) with copper(I) complexes, either $[(TMPA)Cu^I(MeCN)]^+$ (TMPA = tris(2-pyridylmethyl)amine) or $[(MePY2)Cu^I(MeCN)]^+$ (MePY2 = *N*,*N*-bis[2-(2-pyridyl)ethyl]methylamine).[47−51] More recent efforts have focused on their analogous binucleating ligand systems (i.e., "tethered", see diagram), wherein a tetradentate (in the case of $[(^6L)Fe^{II}Cu^I]^+$ [52]) or tridentate (as in $[(^4L)Fe^{II}Cu^I]^+$ [53]) chelate for copper is covalently appended to the periphery of a 2,6-difluorophenyl-substituted porphyrinate. For all cases, Fe^{II}-Cu^I/O_2-reactivity studies reveal the presence of interesting O_2-intermediates detected by low-temperature spectral studies and/or stopped-flow spectrophotometry. Notably, in the case of the tetradentate system $[(^6L)Fe^{II}Cu^I]^+$, a unique high-spin heme-copper peroxo complex, $[(^6L)Fe^{III}$-(O_2^{2-})-$Cu^{II}]^+$,[52] has been extensively characterized, with a similar μ-peroxo species formed in the untethered analogue, $[(F_8TPP)Fe^{III}$-(O_2^{2-})-$Cu^{II}(TMPA)]^+$.[54] Similar O_2-intermediates, including heme-peroxo-Cu species, are observed when tridendate copper chelates are employed, as in (F_8TPP)-$Fe^{II}/[(MePY2)Cu^I(MeCN)]^+$ [51] and its tethered analogue $[(^4L)Fe^{II}Cu^I]^+$.[53]

(10) Gong, W.; Hao, B.; Chan, M. K. *Biochemistry* **2000**, *39*, 3955−3962.
(11) Rodgers, K. R.; Lukat-Rodgers, G. S.; Tang, L. *J. Biol. Inorg. Chem.* **2000**, *5*, 642−654.
(12) Aono, S.; Honma, Y.; Ohkubo, K.; Tawara, T.; Kamiya, T.; Nakajima, H. *J. Inorg. Biochem.* **2000**, *82*, 51−56.
(13) Lanzilotta, W. N.; Schuller, D. J.; Thorsteinsson, M. V.; Kerby, R. L.; Roberts, G. P.; Poulos, T. L. *Nat. Struct. Biol.* **2000**, *7*, 876−880.
(14) Aono, S.; Nakajima, H. *Coord. Chem. Rev.* **1999**, *190*−*192*, 267−282.
(15) Miranda, K. M.; Espey, M. G.; Jourd'heuil, D.; Grisham, M. B.; Fukuto, J. M.; Feelisch, M.; Wink, D. A. *Nitric Oxide* **2000**, 41−55.
(16) Denninger, J. W.; Marletta, M. A. *Biochim. Biophys. Acta* **1999**, *1411*, 334−350.
(17) Sono, M.; Roach, M. P.; Coulter, E. D.; Dawson, J. H. *Chem. Rev.* **1996**, *96*, 2841−2887.
(18) Ortiz de Montellano, P. R. *Cytochrome P-450: Structure, Mechanism and Biochemistry*, 2nd ed.; Plenum: New York, 1995.
(19) Valentine, J. S.; Wertz, D. L.; Lyons, T. J.; Liou, L.-L.; Goto, J. J.; Gralla, E. B. *Curr. Opin. Chem. Biol.* **1998**, *2*, 253−262.
(20) *Active Oxygen in Biochemistry*; Valentine, J. S., Foote, C. S., Greenberg, A., Liebman, J. F., Eds.; Chapman & Hall: New York, 1995.
(21) Schlichting, I.; Berendzen, J.; Chu, K.; Stock, A. M.; Maves, S. A.; Benson, D. E.; Sweet, B. M.; Ringe, D.; Petsko, G. A.; Sligar, S. G. *Science* **2000**, *287*, 1615−1622.
(22) Yano, J. K.; Koo, L. S.; Schuller, D. J.; Li, H. Y.; Ortiz de Montellano, P. R.; Poulos, T. L. *J. Biol. Chem.* **2000**, *275*, 31086−31092.
(23) DuBois, J. L.; Mizoguchi, T. J.; Lippard, S. J. *Coord. Chem. Rev.* **2000**, *200*, 443−485.
(24) Que, L., Jr. *J. Chem. Soc., Dalton Trans.* **1997**, 3933−3940.
(25) Karlin, K. D.; Zuberbühler, A. D. In *Bioinorganic Catalysis*, 2nd ed.; Reedijk, J., Bouwman, E., Eds.; Marcel Dekker: New York, 1999; pp 469−534.
(26) Karlin, K. D.; Kaderli, S.; Zuberbühler, A. D. *Acc. Chem. Res.* **1997**, *30*, 139−147.
(27) Blackman, A. G.; Tolman, W. B. *Struct. Bond.* **2000**, *97*, 179−211.
(28) Suzuki, M.; Furutachi, H.; Okawa, H. *Coord. Chem. Rev.* **2000**, *200*−*202*, 105−129.
(29) Schindler, S. *Eur. J. Inorg. Chem.* **2000**, 2311−2326.
(30) Holmes, M. A.; Trong, I. L.; Turley, S.; Sieker, L. C.; Stenkamp, R. E. *J. Mol. Biol.* **1991**, *218*, 583−593.
(31) Mizoguchi, T. J.; Lippard, S. J. *J. Am. Chem. Soc.* **1996**, *118*, 11022−11023.
(32) Stenkamp, R. E. *Chem. Rev.* **1994**, *94*, 715−726.
(33) Magnus, K. A.; Ton-That, H.; Carpenter, J. E. *Chem. Rev.* **1994**, *94*, 727−735.
(34) Solomon, E. I.; Sundaram, U. M.; Machonkin, T. E. *Chem. Rev.* **1996**, *96*, 2563−2605.
(35) Yoshikawa, S.; Shinzawa-Itoh, K.; Nakashima, R.; Yaono, R.; Yamashita, E.; Inoue, N.; Yao, M.; Jei-Fei, M.; Libeu, C. P.; Mizushima, T.; Yamaguchi, H.; Tomizaki, T.; Tsukihara, T. *Science* **1998**, *280*, 1723−1729.
(36) Ostermeier, C.; Harrenga, A.; Ermler, U.; Michel, H. *Proc. Natl. Acad. Sci. U.S.A.* **1997**, *94*, 10547−10553.
(37) Babcock, G. T. *Proc. Natl. Acad. Sci., U.S.A.* **1999**, *96*, 12971−12973.
(38) Ferguson-Miller, S.; Babcock, G. T. *Chem. Rev.* **1996**, *96*, 2889−2907.
(39) Gennis, R. B. *Proc. Natl. Acad. Sci. U.S.A.* **1998**, *95*, 12747−12749.
(40) Michel, H.; Behr, J.; Harrenga, A.; Kannt, A. *Annu. Rev. Biophys. Biomol. Struct.* **1998**, *27*, 329−356.
(41) Blackmore, R. S.; Greenwood, C.; Gibson, Q. H. *J. Biol. Chem.* **1991**, *266*, 19245−19249.
(42) Oliveberg, M.; Malmström, B. G. *Biochemistry* **1992**, *31*, 3560−3563.
(43) Michel, H. *Proc. Natl. Acad. Sci. U.S.A.* **1998**, *95*, 12819−12824.
(44) Verkhovsky, M. I.; Jasaitis, A.; Verkhovskaya, M. L.; Morgan, J. E.; Wikström, M. *Nature* **1999**, *400*, 480−483.
(45) Wikström, M. *Biochim. Biophys. Acta* **2000**, *1458*, 188−198.
(46) Blomberg, M. R. A.; Siegbahn, P. E. M.; Babcock, G. T.; Wikström, M. *J. Am. Chem. Soc.* **2000**, *122*, 12848−12858.
(47) Karlin, K. D.; Nanthakumar, A.; Fox, S.; Murthy, N. N.; Ravi, N.; Huynh, B. H.; Orosz, R. D.; Day, E. P. *J. Am. Chem. Soc.* **1994**, *116*, 4753−4763.
(48) Nanthakumar, A.; Fox, S.; Murthy, N. N.; Karlin, K. D.; Ravi, N.; Huynh, B. H.; Orosz, R. D.; Day, E. P.; Hagen, K. S.; Blackburn, N. J. *J. Am. Chem. Soc.* **1993**, *115*, 8513−8514.
(49) Nanthakumar, A.; Fox, S.; Karlin, K. D. *J. Chem. Soc., Chem. Commun.* **1995**, 499−501.
(50) Nanthakumar, A.; Fox, S.; Murthy, N. N.; Karlin, K. D. *J. Am. Chem. Soc.* **1997**, *119*, 3898−3906.
(51) Kopf, M.-A.; Neuhold, Y.-M.; Zuberbühler, A. D.; Karlin, K. D. *Inorg. Chem.* **1999**, *38*, 3093−3102.
(52) Ghiladi, R. A.; Ju, T. D.; Lee, D.-H.; Moënne-Loccoz, P.; Kaderli, S.; Neuhold, Y.-M.; Zuberbühler, A. D.; Woods, A. S.; Cotter, R. J.; Karlin, K. D. *J. Am. Chem. Soc.* **1999**, *121*, 9885−9886.
(53) Kopf, M.-A.; Karlin, K. D. *Inorg. Chem.* **1999**, *38*, 4922−4923.
(54) Ghiladi, R. A.; Hatwell, K. R.; Karlin, K. D.; Huang, H.-w.; Moënne-Loccoz, P.; Krebs, C.; Huynh, B. J.; Marzilli, L. A.; Cotter, R. J.; Kaderli, S.; Zuberbühler, A. D. *J. Am. Chem. Soc.* **2001**, *123*, 6183−6184.

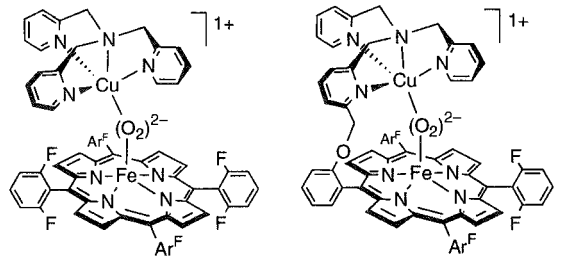

$[(F_8TPP)Fe^{III}–(O_2^{2-})–Cu^{II}(TMPA)]^+$ $[(^6L)Fe^{III}–(O_2^{2-})–Cu^{II}]^+$

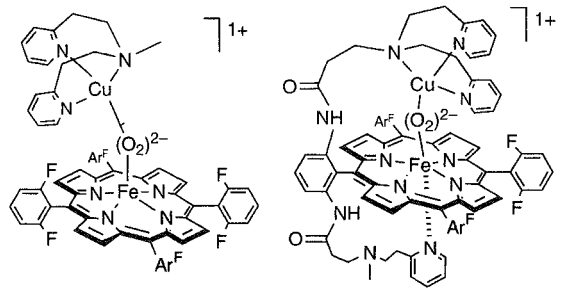

$[(F_8TPP)Fe^{III}–(O_2^{2-})–Cu^{II}(MePY2)]^+$ $[(^4L)Fe^{III}–(O_2^{2-})–Cu^{II}]^+$

Our previous studies on the Cu^I/O_2 chemistry of $[(TMPA)Cu^I(MeCN)]^+$ [26,55] and $[(MePY2)Cu^I(MeCN)]^+$ [56,57] gave us considerable insight into the O_2-complexes involved. However, to fully understand the nature of both the "tethered" and "untethered" synthetic heme-copper/O_2 reactions described above, we need to deduce the O_2-chemistry of $(F_8TPP)Fe^{II}$ (**1**) itself, with a very similar moiety (i.e., with three instead of four 2,6-difluorophenyl meso groups) occurring in ^{6}L or ^{4}L.

Thus, a detailed study of $(F_8TPP)Fe^{II}$ (**1**)/O_2 chemistry is the focus of the present report. First, the X-ray structure of $(F_8TPP)Fe^{II}$ (**1**), as a toluene solvate, is presented, followed by the details of our low-temperature UV−visible and ^{1}H, ^{2}H, and ^{19}F NMR spectroscopic monitoring of the **1**/O_2 chemistry. While following closely the approaches and methods used in the elegant studies by Balch, co-workers, and collaborators,[58−64] we find that the 2,6-difluorophenyl substitution provides interesting behavior contrasting the heme/O_2 chemistry seen for the well-studied tetraphenyl (TPP) or tetramesityl (TMP) porphyrinates. In weakly to moderately coordinating polar solvents, we find that O_2-binding to **1** giving $(F_8TPP)Fe^{III}$-(O_2^-) (**2**) is nicely reversible, and we describe UV−visible-monitored stopped-flow studies which provide kinetic and equilibrium data. Heme-superoxo species such as **2** have been postulated to form during the initial reaction of dioxygen with the heme-copper complexes $(F_8TPP)Fe^{II}/[(TMPA)Cu^I(MeCN)]^+$ [54] and $[(^6L)Fe^{II}$-$Cu^I]^+$,[52] prior to their forming heme-peroxo-Cu adducts. Additionally, **2** is suggested to form as an intermediate in the $(F_8TPP)Fe^{II}/[(MePY2)Cu^I(MeCN)]^+$ [51] oxygenation reaction and may well be present during O_2-binding to $[(^4L)Fe^{II}Cu^I]^+$.[53] In contrast to the superoxo dominated chemistry found in coordinating solvents, the reaction of $(F_8TPP)Fe^{II}$ (**1**) with dioxygen in nonpolar solvents leads to a μ-peroxo dinuclear complex, $[(F_8TPP)Fe^{III}]_2$-(O_2^{2-}) (**3**); the *reversibility* of this reaction represents an interesting finding not previously observed. Finally, as also studied by Balch and co-workers,[61] we describe the addition of ligand base to **3**, thereby cleaving the O−O bond and affording the high-valent iron(IV) oxo complex (F_8TPP)-Fe^{IV}═O (**4**). The spectroscopic characterization of this "ferryl" species with the F_8TPP porphyrin system may be potentially important for a detailed understanding of our heme-copper oxidase model studies (i.e., $[(^6L)Fe^{II}Cu^I]^+$ or $[(^4L)Fe^{II}Cu^I]^+$; vide supra), since heme-copper oxidases afford ferryl (**P**)Fe^{IV}═O intermediates during the $4e^-/4H^+$ reduction of dioxygen to water.[37,39,43−45]

Results and Discussion

Synthesis. Procedures for making the free base F_8TPPH_2,[47,51,65] ferric chloride $(F_8TPP)Fe^{III}$-Cl,[47] and target $(F_8TPP)Fe^{II}$ (**1**)[51] porphyrin complexes have been previously described, but modified synthetic procedures are presented here. The structures of both the $(F_8TPP)Fe^{III}$-Cl precursor complex and $(F_8TPP)Fe^{II}$ (**1**) were determined by X-ray crystallography; discussion of the structure of $(F_8TPP)Fe^{II}$ (**1**) is found below, while the unremarkable structure of $(F_8TPP)Fe^{III}$-Cl can be found in the Supporting Information.

To simplify the interpretation of NMR spectra, a pyrrole-deuterated analogue of **1**, $(F_8TPP$-$d_8)Fe^{II}$ (**1**-d_8),[51] was synthesized, thereby allowing for ^{2}H NMR spectroscopic monitoring of low-temperature stable dioxygen adducts with unambiguous assignment of the pyrrole resonances. The synthesis employed in deuteration of the pyrrole hydrogens is similar to the ones reported earlier in the literature,[66] affording F_8TPPH_2 with greater than 90% (by mass spectrometric analysis) deuterium incorporation into the eight β-pyrrole hydrogen positions. This route was deemed necessary given the ability to assign oxidation and spin states of hemes, as well as the types of heme/O_2-adducts formed, based upon the chemical shift of the pyrrole hydrogens.[67−69]

X-ray Structure of 1·(C_7H_8)$_2$. Experimental data for the X-ray structure data collection and analysis for **1** are given in Table 1 and the Supporting Information. The structure of $(F_8TPP)Fe^{II}$·$(C_7H_8)_2$ (**1**·$(C_7H_8)_2$), as the bis(toluene) solvate, is shown in Figure 1. Compound **1**·$(C_7H_8)_2$ is a mononuclear, tetracoordinate iron(II) species, with ligation to the four pyrrole nitrogens. The geometry around the ferrous ion is square planar (with the iron lying in the plane of the porphyrin macrocycle) [∠N−Fe−N (all) = 90.0°, Fe−N_4 (av) = 2.002 Å]. This is comparable to other four-coordinate metalloporphyrins,[70] most

(55) Tyeklár, Z.; Jacobson, R. R.; Wei, N.; Murthy, N. N.; Zubieta, J.; Karlin, K. D. *J. Am. Chem. Soc.* **1993**, *115*, 2677−2689.
(56) Liang, H.-C.; Karlin, K. D.; Dyson, R.; Kaderli, S.; Jung, B.; Zuberbühler, A. D. *Inorg. Chem.* **2000**, *39*, 5884−5894.
(57) Obias, H. V.; Lin, Y.; Murthy, N. N.; Pidcock, E.; Solomon, E. I.; Ralle, M.; Blackburn, N. J.; Neuhold, Y.-M.; Zuberbühler, A. D.; Karlin, K. D. *J. Am. Chem. Soc.* **1998**, *120*, 12960−12961.
(58) Balch, A. L.; Chan, Y.-W.; Cheng, R.-J.; La Mar, G. N.; Latos-Grazynski, L.; Renner, M. W. *J. Am. Chem. Soc.* **1984**, *106*, 7779−7785.
(59) Balch, A. L. *Inorg. Chim. Acta* **1992**, *198*−*200*, 297−307.
(60) Chin, D.-H.; La Mar, G. N.; Balch, A. L. *J. Am. Chem. Soc.* **1980**, *102*, 4344−4350.
(61) Chin, D.-H.; Balch, A. L.; La Mar, G. N. *J. Am. Chem. Soc.* **1980**, *102*, 1446−1448.
(62) Chin, D.-H.; La Mar, G. N.; Balch, A. L. *J. Am. Chem. Soc.* **1980**, *102*, 5945−5947.
(63) La Mar, G. N.; de Ropp, J. S.; Latos-Grazynski, L.; Balch, A. L.; Johnson, R. B.; Smith, K. M.; Parish, D. W.; Cheng, R.-J. *J. Am. Chem. Soc.* **1983**, *105*, 782−787.
(64) Latos-Grazynski, L.; Cheng, R.-J.; La Mar, G. N.; Balch, A. L. *J. Am. Chem. Soc.* **1982**, *104*, 5992−6000.
(65) Nanthakumar, A.; Goff, H. M. *Inorg. Chem.* **1991**, *30*, 4460−4464.
(66) Shirazi, A.; Goff, H. M. *J. Am. Chem. Soc.* **1982**, *104*, 6318−6322.
(67) Goff, H. M.; La Mar, G. N. *J. Am. Chem. Soc.* **1977**, *99*, 6599−6606.
(68) Walker, F. A.; Simonis, U. In *Biological Magnetic Resonance*; Berliner, L. J., Reuben, J., Eds.; Plenum Press: New York, 1993; Vol. 12/ NMR of Paramagnetic Molecules, pp 133−274.
(69) Walker, F. A. In *The Porphyrin Handbook*; Kadish, K. M., Smith, K. M., Guilard, R., Eds.; Academic Press: San Diego, 2000; Vol. 5/NMR and EPR, pp 81−184.

Table 1. Crystal Data and Structure Refinement for $(F_8TPP)Fe^{II}\cdot(C_7H_8)_2$ (**1**·$(C_7H_8)_2$)

empirical formula	$C_{58}H_{36}F_8FeN_4$
fw	996.76
temperature	195(2) K
wavelength	0.71073 Å
cryst syst	monoclinic
space group	*C*2/*c*
unit cell dimens	$a = 20.9177(2)$ Å, $\alpha = 90°$ $b = 11.7738(2)$ Å, $\beta = 108.6999(6)°$ $c = 19.3875(2)$ Å, $\gamma = 90°$
volume, *Z*	4522.71(9) Å^3, 4
density (calcd)	1.464 g/cm^3
abs coeff	0.413 mm^{-1}
F(000)	2040
cryst size	0.50 × 0.50 × 0.10 mm
cryst color	red plate
θ range for data collection	2.01−28.18°
limiting indices	$-24 \le h \le 26$, $-13 \le k \le 15$, $-23 \le l \le 24$
no. of reflns collected	14 417
no. of ind reflns	5251 ($R_{int} = 0.0285$)
refinement method	full-matrix least-squares on F^2
no. of data/restraints/params	5251/0/322
goodness-of-fit on F^2	1.006
final *R* indices [$I > 2\sigma(I)$]	$R_1 = 0.0421$, $wR_2 = 0.1005$
R indices (all data)	$R_1 = 0.0576$, $wR_2 = 0.1102$
largest diff peak and hole	0.385 and −0.459 e Å^{-3}

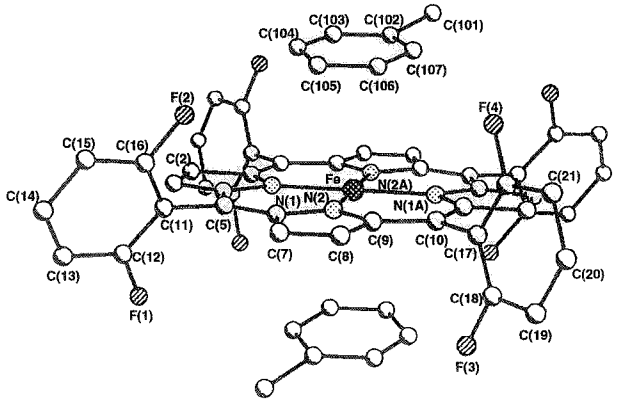

Figure 1. Perspective view (30% ellipsoids) of the structure of **1**·$(C_7H_8)_2$. Selected bond lengths (Å) and angles (deg): Fe−N_4(av) = 2.002, ∠N−Fe−N (all) = 90.0, Fe−C(105) = 3.149, Fe−C(106) = 3.112.

notably $(TPP)Fe^{II}$, which has an average Fe−N distance of 1.972 Å and ∠N−Fe−N (av) = 90.0°.[71]

The asymmetric unit consists of half of **1**·$(C_7H_8)_2$ located on an inversion center and a molecule of toluene, for an overall stoichiometry of two toluenes per ferrous heme, one π-stacked above the plane of the porphyrin macrocycle, the other below (Figure 1). The stacked toluenes are nearly coplanar with the porphyrin macrocycle, with a small angle of 10.2° between the two planes. Weak axial interactions between the ferrous ion and two carbon atoms of each toluene appear to exist, with distances of 3.149 and 3.112 Å for Fe−C(105) and Fe−C(106), respectively. Such interactions between hemes and aromatic solvates are known in other M^{II} or Fe^{III} porphyrinates,[72−76] and relevant data for arene solvates of several metalloporphyrins are given in Table 2.

The one unique feature of $(F_8TPP)Fe^{II}\cdot(C_7H_8)_2$ (**1**·$(C_7H_8)_2$), when compared to the other metalloporphyrins in Table 2, is that the closest M···C_{arene} contact is to a meta-carbon of the toluene solvate. In all other cases, the closest metal−solvate distance is to an electron-rich ortho- or para-arene carbon atom, with the metal center acting as an electron acceptor.[75] Given that the fluorine substituents in $(F_8TPP)Fe^{II}$ (**1**) should make the ferrous ion an even better electron acceptor compared to the unsubstituted TPP, it is somewhat surprising to see that the closest metal−toluene contact in **1**·$(C_7H_8)_2$ is to the more electron-deficient meta carbon. Furthermore, the crystal structure shows that the 2,6-difluorophenyl groups on the meso carbon positions are not perpendicular to the porphyrin plane; one pair of opposing 2,6-difluorophenyl rings is rotated by an angle of 8.1° from perpendicularity, while for the other pair, this angle is −20.8° (i.e., twisted in the opposite direction).

Solvent-Dependent Spin State of $(F_8TPP)Fe^{II}$ (1). Depending upon the solvent, multiple Fe^{II} spin states are observed for **1**, as detected by ^{1,2}H NMR spectroscopy. Table 3 shows the chemical shifts of the pyrrole hydrogens of $(F_8TPP)Fe^{II}$ (**1**) in various solvents at 293 and 193 K, along with their corresponding Evans method magnetic moment measurements (293 K). In noncoordinating solvents, such as methylene chloride or toluene, the pyrrole hydrogen resonances are found at ∼δ 3.9−4.9 ppm. This has been previously characterized for **1** as a four-coordinate heme in an $S = 1$ spin state,[49] with the ferrous ion in the plane of the porphyrin (as also shown by the crystal structure of **1**). Consistent with this intermediate spin-state formulation was the finding of $\mu_B = 3.0$, close to the spin-only value of 2.8 for two unpaired electrons.

In weakly to moderately coordinating solvents, such as acetone and tetrahydrofuran (THF), these pyrrole-H resonances are paramagnetically shifted downfield, to δ 48 (acetone) and δ 56 (THF) ppm. This is indicative of a high-spin ferrous ($S = 2$) complex,[68,69,77] with axial solvent ligation, either as a five-coordinate heme (moderate axial field ligands, i.e., acetone) or as a six-coordinate heme (i.e., two weak-field axial THF ligands).[78,79] The Evans method magnetic moment measurements now show a $\mu_B = 5.0-5.1$, consistent with a high-spin $S = 2$ system having four unpaired electrons ($\mu_B = 4.9$; spin-only value). In MeCN solvent, however, the pyrrole hydrogens were found at δ 28 ppm [$\mu_B = 4.1$; Evans method, 293 K] and are representative of an equilibrium mixture of high- and low-spin states. Upon lowering the MeCN solution to 233 K, the pyrrole hydrogens displayed anti-Curie behavior as they shifted upfield to δ 10.1 ppm, indicating more complete formation of a low-spin six-coordinate heme. This temperature-dependent behavior is consistent with the spin-equilibrium proposed of a high-spin (five-coordinate, one axially bound MeCN) structure favored at higher temperature and a low-spin (six-coordinate, two axially bound MeCN) structure favored at lower temperatures.

Finally, in a strongly coordinating solvent such as pyridine, the pyrrole resonances are found at δ 8.9 ppm; a diamagnetic

(70) Senge, M. O. In *The Porphyrin Handbook*; Kadish, K. M., Smith, K. M., Guilard, R., Eds.; Academic Press: San Diego, 2000; Vol. 10.
(71) Collman, J. P.; Hoard, J. L.; Kim, N.; Lang, G.; Reed, C. A. *J. Am. Chem. Soc.* **1975**, *97*, 2676−2681.
(72) Kirner, J. F.; Reed, C. A.; Scheidt, W. R. *J. Am. Chem. Soc.* **1977**, *99*, 1093−1101.
(73) Scheidt, W. R.; Reed, C. A. *Inorg. Chem.* **1978**, *17*, 710−714.
(74) Scheidt, W. R.; Kastner, M. E.; Hatano, K. *Inorg. Chem.* **1978**, *17*, 706−710.
(75) Shelly, K.; Bartczak, T.; Scheidt, W. R.; Reed, C. A. *Inorg. Chem.* **1985**, *24*, 4325−4330.
(76) Xie, Z.; Bau, R.; Reed, C. A. *Angew. Chem., Int. Ed. Engl.* **1994**, *33*, 2433−2434.
(77) La Mar, G. N.; Walker, F. A. In *The Porphyrins*; Dolphin, D., Ed.; Academic Press: 1979; Vol. IVB, pp 57−161.
(78) Reed, C. A.; Mashiko, T.; Scheidt, W. R.; Spartalian, K.; Lang, G. *J. Am. Chem. Soc.* **1980**, *102*, 2302−2306.
(79) Thompson, D. W.; Kretzer, R. M.; Lebeau, E. L.; Scaltrio, D.; Ghiladi, R. A.; Lam, K.-C.; Rheingold, A. L.; Meyer, G. J.; Karlin, K. D. Manuscript in preparation.

Table 2. Summary of Metalloporphyrin−Arene Contacts.

	$(F_8TPP)Fe^{II}$ [a]	(TPP)Cr[a]	(TPP)Zn[a]	(TPP)Mn[a]	$[(TPP)Fe]^+$ [b]	$[(TPP)Fe]^+$ [c]
interplanar spacing, Å		3.37	3.34	3.30	3.30	
interplanar angle, deg	10.2	4.5	12.0	10.7	7.0	13.0
closest $M\cdots C_{arene}$ contact, Å	3.11	3.36	3.12	3.05	3.34	2.94
carbon atom type	meta	ortho	para	para	ortho	ortho
reference	this work	73	74	72	75	76

[a] Toluene solvate. [b] Fluorobenzene solvate. [c] *p*-Xylene solvate.

Table 3. Chemical Shifts of the Pyrrole Hydrogens at 293 and 193 K and Their Corresponding Magnetic Moments (Evans Method, 293 K) in Various Solvents.

	solvent					
	THF	acetone	acetonitrile	CH_2Cl_2	toluene	pyridine
$\delta_{pyrrole}$ (293 K), ppm	56	48	28	4.9	3.9	8.9
$\delta_{pyrrole}$ (193 K), ppm	93	84	10.1 (233 K)	−2.5		
μ_B (293 K)	5.1	5.0	4.1	3.0		0

Scheme 1

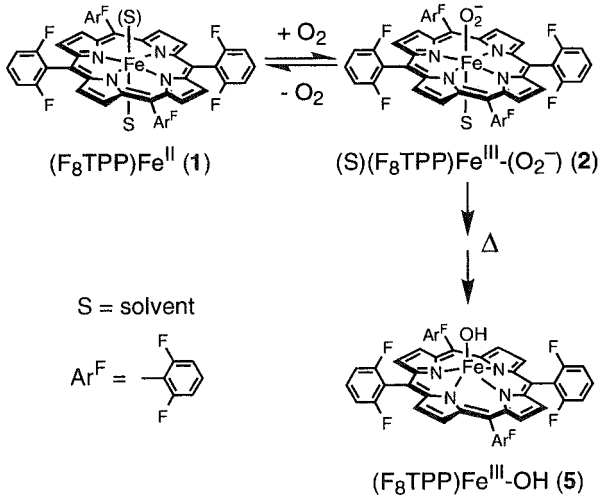

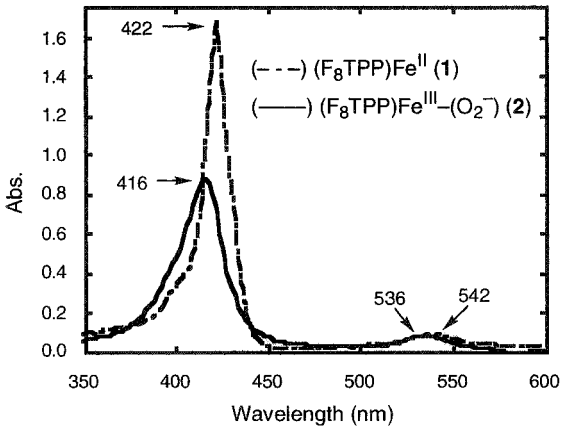

Figure 2. UV−visible spectra of the $(F_8TPP)Fe^{II}$ (**1**)/$(F_8TPP)Fe^{III}$-(O_2^-) (**2**) reversible dioxygenation reaction in THF at 193 K. See text for further discussion.

NMR spectrum is observed, suggesting a six-coordinate, low-spin ferrous center ($S = 0$, low-spin d^6) with strong axial ligation by two pyridine ligands. As expected, an Evans method NMR experiment shows $\mu_B = 0$; that is, no paramagnetically shifted solvent peak was observed downfield from the reference/capillary solvent resonance.

Reversible Iron-Superoxo Formation: (S)$(F_8TPP)Fe^{III}$-(O_2^-) (2). UV−Visible Spectroscopy. Low-temperature UV−visible spectroscopic monitoring of the $(F_8TPP)Fe^{II}$ (**1**)/O_2 reaction in coordinating solvents reveals the presence of a reversibly formed intermediate, **2**, which was found to be stable indefinitely at 193 K. Ultimately, thermal decomposition to the previously characterized[47] ferric hydroxy complex, $(F_8TPP)Fe^{III}$-OH (**5**), occurs upon warming (Scheme 1).

The reduced $(F_8TPP)Fe^{II}$ (**1**) complex exhibits UV−visible features at 422 (Soret) and 542 nm in THF solvent at 193 K (Figure 2 and Figure S1). Upon bubbling dioxygen directly through the solution thereby forming **2**, an immediate change in the spectrum is observed [λ_{max} = 416 (Soret), 536 nm]. Formation of **2** is not limited to THF solvent, however, as similar chemistry is observed when the oxygenation reaction is performed in EtCN (193 K). Here, addition of O_2 to $(F_8TPP)Fe^{II}$ (**1**) [λ_{max} = 414, 424 (split Soret), 526 nm] results in a new spectrum [λ_{max} = 414 nm (Soret), 536 nm] (Figure S2).

Upon bubbling argon through the solution containing the heme-O_2 complex **2** at 193 K, it was possible to reverse the dioxygen-binding and give back (with only minor decomposition to **5**) the starting complex, reduced species $(F_8TPP)Fe^{II}$ (**1**). Figures S1 and S2 show this cycling as followed by UV−visible spectroscopy, in THF and EtCN solvents, respectively. Evolution of O_2 by this process was confirmed by using alkaline pyrogallol, which was employed as a means for detecting liberated dioxygen (see Experimental Section). Interestingly, application of a simple vacuum without the Ar bubbling purge was not able to reverse the dioxygen adduct back to the reduced complex at low temperature. Additional discussion pertaining to the reversibility of **2** can be found in the Supporting Information.

Dioxygen-uptake manometry in THF at 193 K revealed a reaction stoichiometry of 1 Fe:1.02 O_2 (see Experimental Section), confirming the proposed formation of a myoglobin-like iron(III)-superoxo complex, (S)$(F_8TPP)Fe^{III}$-(O_2^-) (**2**), where S represents a coordinated axial base solvent molecule (Scheme 1).

The reversibility of O_2-binding to $(F_8TPP)Fe^{II}$ (**1**) was also demonstrated employing acetone as solvent; these observations (UV−visible and ^2H NMR spectroscopies) are reported in the Supporting Information, Figures S3−S5.

NMR Spectroscopic Characterization of (S)$(F_8TPP$-$d_8)$-Fe^{III}-(O_2^-) (2-d_8). Figure 3 depicts a typical low-temperature oxygenation reaction of **1**-d_8 in THF solvent, as monitored by ^2H NMR spectroscopy. Complex $(F_8TPP$-$d_8)Fe^{II}$ (**1**-d_8) gives rise to a high-spin (vida supra) pyrrole resonance at δ 56 ppm (Figure 3a, 293 K). The expected temperature-dependent paramagnetic downfield-shifting of the pyrrole resonance to δ 93 ppm is seen at 193 K (Figure 3b). Upon generation of the dioxygen intermediate, **2**, by bubbling O_2 via syringe directly

Table 4. NMR Data and Pyrrole Chemical Shifts of Heme-Superoxo {PFe^{III}-(O_2^-)}, Heme-Peroxo-Heme {(PFe^{III})$_2$-(O_2^{2-})}, and Ferryl {PFe^{IV}=O} Complexes

complex	$\delta_{pyrrole}$	solvent	temp (K)	ref
(THF)(F_8TPP-d_8)Fe^{III}-(O_2^-) (**2**-d_8)	8.9	THF	193	this work
(acetone)(F_8TPP-d_8)Fe^{III}-(O_2^-) (**2**-d_8)	8.9	acetone	193	this work
(N-MeIm)(TMP)Fe^{III}-(O_2^-)	8.37	toluene-d_8	196	58
(TpivPP)Fe^{II}I-(O_2^-)[a]	8.2	toluene-d_8	197	64
(T(2,4,6-MeO)$_3$PP)Fe^{III}-(O_2^-)[a]	9.0	CD_2Cl_2	198	64
(T(2,4,6-EtO)$_3$PP)Fe^{III}-(O_2^-)[a]	9.1	CD_2Cl_2	198	64
(T(3,4,5-MeO)$_3$PP)Fe^{III}-(O_2^-)[a]	9.8	toluene-d_8	198	64
[(F_8TPP-d_8)Fe^{III}]$_2$-(O_2^{2-}) (**3**-d_8)	17.5	CH_2Cl_2	193	this work
[(TMP)Fe^{III}]$_2$-(O_2^{2-})	17.7, 19.0	toluene-d_8	203, 243	58
[(TPP)Fe^{III}]$_2$-(O_2^{2-})	16.0	toluene-d_8	193	60
[(TpivPP)Fe^{III}]$_2$-(O_2^{2-})	16.6	toluene-d_8	248	64
[(TmTP)Fe^{III}]$_2$-(O_2^{2-})	16.2	toluene-d_8	193	60
[(DPDMe)Fe^{III}]$_2$-(O_2^{2-})	19.2	toluene-d_8	199	60
[(T(3,4,5-MeO)$_3$PP)Fe^{III}]$_2$-(O_2^{2-})	16.8	toluene-d_8	243	64
(DMAP)(F_8TPP-d_8)Fe^{IV}=O (**4**-d_8)	3.5	CH_2Cl_2	193	this work
(TMP)Fe^{IV}=O	8.4	toluene-d_8	203	58
(THF)(TpivPP)Fe^{IV}=O	7.2	THF-d_8	223	96
(1-MeIm)(TPP)Fe^{IV}=O	5.05	toluene-d_8	193	58
(1-MeIm)(TmTP)Fe^{IV}=O	~5	toluene-d_8	200	61
(1-MeIm)(TMP)Fe^{IV}=O	4.6	toluene-d_8	243	58

[a] Denotes five-coordinate, diamagnetic complex due to lack of a suitable axial base; TMP = *meso*-tetramesitylporphyrin dianion; TpivPP = *meso*-tetrakis(α,α,α,α-*o*-pivalamidophenyl)porphyrin dianion; T(2,4,6-MeO)$_3$PP = *meso*-tetrakis(2,4,6-trimethoxyphenyl)porphyrin dianion; T(2,4,6-EtO)$_3$PP = *meso*-tetrakis(2,4,6-triethoxyphenyl)porphyrin dianion; T(3,4,5-MeO)$_3$PP = *meso*-tetrakis(3,4,5-trimethoxyphenyl)porphyrin dianion; TPP = *meso*-tetraphenylporphyrin; TmTP = *meso*-tetra-*m*-tolylporphyrin; DPDMe = deuterioporphyrin IX dimethyl ester; DMAP = 4-(dimethylamino)pyridine; N-MeIm = 1-MeIm = *N*-methylimidazole.

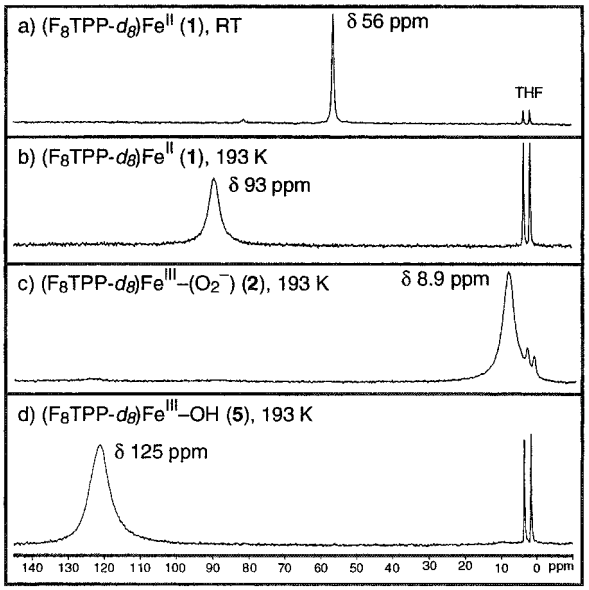

Figure 3. ^{2}H NMR spectra of the (F_8TPP-d_8)Fe^{II} (**1**-d_8) oxgyenation reaction in THF at 193 K. See text for explanation.

into an NMR tube containing **1** in a dry ice/acetone bath, a diamagnetic spectrum is observed ($\delta_{pyrrole}$ = 8.9 ppm) (Figure 3c), consistent with the formulation of (THF)(F_8TPP)Fe^{III}-(O_2^-) (**2**) and possessing a low-spin (S = 0) six-coordinate iron. This ^{2}H NMR-derived pyrrole-H resonance assignment is in agreement with previously studied five- and six-coordinate diamagnetic heme-superoxo complexes (Table 4). Warming the solution of **2** to room temperature (several hours) leads to complete formation of (F_8TPP-d_8)Fe^{III}-OH (**5**-d_8) ($\delta_{pyrrole}$ = 125 ppm, 193 K) (Figure 3d).

Using the assigned pyrrole hydrogen resonances in the ^{2}H NMR spectrum of **2**-d_8 (THF, 193 K), we are able to exclude the possibility of **2** being the intermolecular μ-peroxo dimer PFe^{III}-OO-Fe^{III}P (~15−17 ppm, 193 K; vide infra),[58,60,64] the high-valent iron-oxo (ferryl) complex PFe^{IV}=O (~2−4 ppm, 193−233 K, vide infra),[58,61] the anionic mononuclear iron

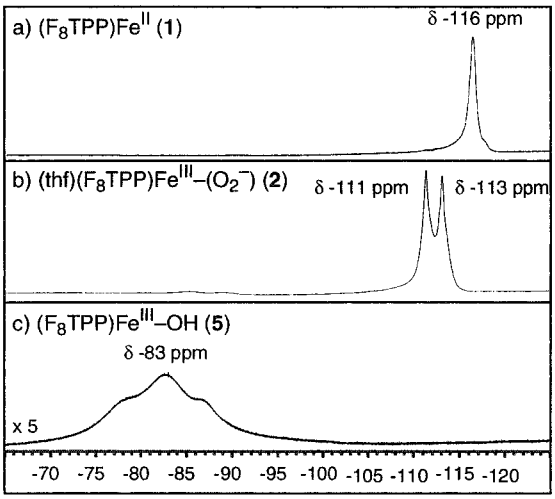

Figure 4. ^{19}F NMR spectra of the oxygenation reaction of (F_8TPP)Fe^{II} (**1**) in THF, 193 K.

peroxide complex [PFe^{III}-O_2]$^-$ (~60 ppm, RT),[66] the intermolecular μ-oxo complex (F_8TPP)Fe^{III}-O−Fe^{III}(F_8TPP) (13.7 ppm, RT),[47] or (F_8TPP)Fe^{III}-OH (**5**) (125 ppm, 193 K).[47]

Additional characterization of the heme-superoxo complex (S)(F_8TPP)Fe^{III}-(O_2^-) (**2**) comes from ^{19}F NMR spectroscopy. (F_8TPP)Fe^{II} (**1**) exhibits a single fluorine resonance at δ −116 ppm (THF, 193 K, Figure 4a), implying a symmetric and equivalent environment for all fluorine substituents in **1** [i.e., a six-coordinate (bis-THF) high-spin ferrous heme].[79] Upon oxygenation, two distinctive fluorine resonances of approximately equal integration appear at δ −111 and −113 ppm (Figure 4b, 193 K). The origin of these two resonances may be due to the asymmetry of **2** (S = THF), with one resonance due to the fluorines located on the superoxo ligand side of the porphyrin plane and the second resonance due to those fluorines on the THF ligand side. This hypothesis is reasonable, since different chemical shifts for inequivalent porphyrin phenyl substituents due to the asymmetry imposed by oxygen and/or axial ligand binding have been shown before by ^{1}H NMR

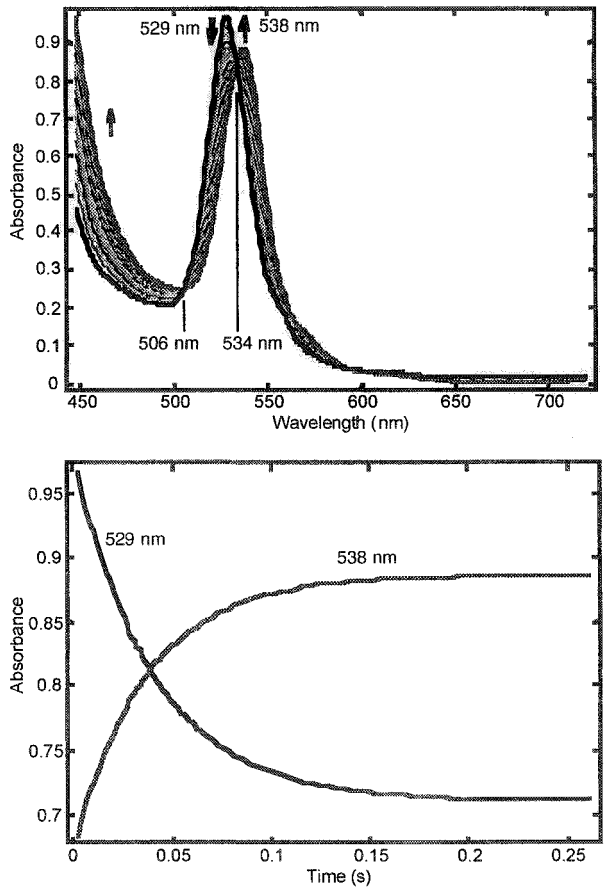

Figure 5. Time-dependent oxygenation of $(F_8TPP)Fe^{II}$ (**1**) ($\lambda_{max} = 529$ nm) in EtCN (183 K, $t_{total} = 250$ ms) (top). Traces for the formation of the 538 nm band ascribed to $(S)(F_8TPP)Fe^{III}$-(O_2^-) (**2**) and loss of the 529 nm band are shown (bottom).

spectroscopy.[58] After warming to room temperature and subsequent rechilling, the decomposition product $(F_8TPP)Fe^{III}$-OH (**5**) was observed (Figure 4c, δ −83 ppm), as confirmed by comparison to a ^{19}F NMR spectrum of authentic material.

Kinetics−Thermodynamics of the Oxygenation of $(F_8TPP)Fe^{II}$ (1) in Coordinating Solvents. Stopped-flow (UV−visible) spectrophotometry studies were able to provide valuble insight into the kinetics and thermodynamics of reversible O_2-binding to $(F_8TPP)Fe^{II}$ (**1**) forming $(S)(F_8TPP)Fe^{III}$-(O_2^-) (**2**) in coordinating solvents such as EtCN and THF.

$$(F_8TPP)Fe^{II}\ (\mathbf{1}) + O_2 \underset{k_{-1}}{\overset{k_1(K_1)}{\rightleftharpoons}} (S)(F_8TPP)Fe^{III}\text{-}(O_2^-)\ (\mathbf{2}) \quad (1)$$

Spectroscopic monitoring of the oxygenation reaction was performed between 450 and 725 nm, allowing for complete resolution of the alpha band region.

For the kinetics of oxygenation of $(F_8TPP)Fe^{II}$ (**1**) in EtCN solvent, data collected over a range 178−205 K were used in the analysis. Figure 5 depicts a typical stopped-flow UV−visible data set obtained at 183 K. Upon oxygenation, loss of the 529 nm band, attributed to $(F_8TPP)Fe^{II}$ (**1**), and formation of the 538 nm band, $(S)(F_8TPP)Fe^{III}$-(O_2^-) (**2**), was observed concurrently ($t_{1/2,183K} \approx 25$ ms); isosbestic points were seen at 506 and 534 nm. The data were fit to a second-order reversible reaction; an Eyring plot is given in the Supporting Information (Figure S6). As can be seen from the results of the analysis provided in Table 5, the equilibrium constant, K_1, for the fully reversible oxygenation reaction is very favorable at low temperature, $6 \times 10^5\ M^{-1}$ at 183 K. However, as expected, at higher T (extrapolated) the reaction becomes less favorable ($\sim 10^1\ M^{-1}$ at 298 K) due to the strongly unfavorable entropic component, $\Delta S° = -105 \pm 23$ J/(K mol). Enthalpies and entropies of activation for the O_2-binding (k_1) and dissociation (k_{-1}) reaction were obtained (Table 5) and are discussed below.

Table 5. Kinetic (k_1, k_{-1}) and Thermodynamic (K_1) Parameters for the Oxygenation of $(F_8TPP)Fe^{II}$ (**1**) in EtCN and THF Solvents

parameter	temp, K	propionitrile	tetrahydrofuran
K_1 (M^{-1})	183	6×10^5	1×10^5
	233	$(6 \pm 1) \times 10^3$	$(1.21 \pm 0.04) \times 10^3$
	293	$(3 \pm 2) \times 10^1$	$(7.4 \pm 0.2) \times 10^0$
$\Delta H°$ (kJ/mol)		-40 ± 5	-37.5 ± 0.4
$\Delta S°$ (J/K mol)		-105 ± 23	-109 ± 2
k_1 ($M^{-1}\ s^{-1}$)	183	$(5.57 \pm 0.04) \times 10^3$	
	233	$(6.4 \pm 0.1) \times 10^5$	
	293	$(1.6 \pm 0.1) \times 10^8$	
$\Delta H^‡$ (kJ/mol)		38.6 ± 0.2	
$\Delta S^‡$ (J/K mol)		42 ± 1	
k_{-1} (s^{-1})	183	9×10^{-3}	
	233	$(1.1 \pm 0.2) \times 10^2$	
	293	$(6 \pm 5) \times 10^6$	
$\Delta H^‡$ (kJ/mol)		78 ± 5	
$\Delta S^‡$ (J/K mol)		147 ± 23	

In THF solvent, the reaction of $(F_8TPP)Fe^{II}$ (**1**) with dioxygen was too fast to be followed by stopped-flow spectrophotometry; that is, full formation of **2** occurred within the mixing time of the apparatus ($\sim$1 ms). However, it was possible to extract equilibrium data (Table 5) for this reversible oxygenation reaction through temperature-dependent studies by analyzing the relative amount of **1** ($\lambda_{max} = 543$ nm) and **2** ($\lambda_{max} = 535$ nm) present in equilibrium at a given T (Figure S7); the van't Hoff plot is provided in the Supporting Information, Figure S8.

Comparison of the thermodynamic parameters obtained for both EtCN and THF solvents shows that $\Delta H°$ and $\Delta S°$ (thus, K values as well) are very similar. This indicates that as axial ligands for $(F_8TPP)Fe^{II}$ (**1**), THF (an oxygen-atom donor) and EtCN (a nitrogen-atom donor) are nearly identical in their effect with respect to formation and stabilization of the heme-superoxo complex $(S)(F_8TPP)Fe^{III}$-(O_2^-) (**2**). This might seem somewhat surprising, given the differences in electronic structure of $(F_8TPP)Fe^{II}$ (**1**) in these two solvents at low temperature: (i) in THF, a six-coordinate high-spin heme ($\delta_{pyrrole} = 93$ ppm) prevails with ferrous ion in the plane of the porphyrin macrocycle;[79] (ii) in EtCN, a six-coordinate, low-spin heme [$\delta_{pyrrole} = 10.1$ ppm (MeCN, 233 K), UV−visible split Soret band in EtCN (Figure S2)] is also diagnostic of a low-spin ferrous heme[80]) with ferrous ion in the porphyrin plane. An explanation may reside in a balancing of different effects in the two solvents: formation of **2** in EtCN with the softer (less favorable) nitrile ligand (for Fe^{III}, yielding an $N-Fe^{III}$ bond) and no spin-state change may be roughly equivalent to forming **2** with a relatively more favorable hard THF ligand (giving an $O-Fe^{III}$ bond), but whose formation is also accompanied by the less favorable spin-state change.

Table 6 shows thermodynamic and kinetic comparisons for O_2-binding (yielding heme-superoxo complexes) of $(F_8TPP)Fe^{II}$ (**1**) with other heme systems. Despite having an extrapolated (room temperature) forward rate constant (k_1) up to 100 times faster in EtCN (possibly due to the lack of steric hindrance for O_2-binding in **1**), the equilibrium constant (K_1) for **1** is smaller (factor of 10^1-10^5). This is presumably due to the electron-withdrawing fluorine substituents, which lead to a weaker Fe−O bond strength upon O_2-binding (hence, the larger k_{-1} for reaction

(80) Gouterman, M. In *The Porphyrins*; Dolphin, D., Ed.; Academic Press: New York, 1978; Vol. 3 (Part A), pp 1−165.

Table 6. Equilibrium and Kinetic Data for Heme-Dioxygen Complexes (20 °C, unless otherwise stated)

compound	k_1, M^{-1} s^{-1}	k_{-1}, s^{-1}	K_1, M^{-1}	$P_{1/2}^{O_2}$, torr	$\Delta H_1^{\ddagger}$, kJ/mol	$\Delta S_1^{\ddagger}$, J/K mol	$\Delta H°$, kJ/mol	$\Delta S°$, J/K mol	ref
(F_8TPP)Fe^{II} (**1**)[a]	$(1.6 \pm 0.1) \times 10^8$	$(6 \pm 5) \times 10^6$	$(3 \pm 2) \times 10^1$		38.6 ± 0.2	42 ± 1	-40 ± 5	-105 ± 23	*c*
(F_8TPP)Fe^{II} (**1**)[b]			$(7.4 \pm 0.2) \times 10^0$				-37.5 ± 0.4	-109 ± 2	*c*
myoglobin	$1-2 \times 10^7$	10−30	4.30×10^8	0.37−1			−64 to −88	−159 to −235	81−83
[Piv_3(5CImP)P]Fe	4.3×10^8	2.9×10^3	1.48×10^5	0.58	0.75 ± 0.33	-116 ± 2.5	-68 ± 3.3	-167 ± 13	82
[Piv_3(4ClmP)P]Fe	4.3×10^8	2.9×10^3	1.48×10^5	0.60			-70 ± 2.1	-176 ± 8.3	82
(T_{piv}PP)Fe(1,2−Me_2Im)	1.06×10^8	4.6×10^4	2.31×10^3	38	10.5 ± 1.6	-95 ± 4	-60 ± 2	-176 ± 8.3	82
(MedPoc)Fe(1-MeIm)	1.7×10^7	71	2.4×10^5	0.36	7.1 ± 2.5	-121 ± 8			82
(PocPiv)Fe(1-MeIm)	2.2×10^6	9	2.4×10^5	0.36	35 ± 2.5	-45 ± 10			82
chelated protoheme	6.2×10^7	4000	1.6×10^4	5.6			−59	−146	82,84,85
(durene-4/4)Fe(1,2-Me_2Im)				2450			−54.8	−190	86
(durene-4/4)Fe(DcIm)	8.2×10^7	10^5	820	139			−64	−207	86
(C_2-cap)Fe(1-MeIm)				23			−44	−117	87,88
(C_2-cap)Fe(1,2-Me_2Im)				4000			−41	−150	87,88
(PocPiv)Fe(1,2-Me_2Im)	1.9×10^6	280	6.8×10^3	12.6					82
(TPP)Fe[(NH(CH_2)$_3$Im]	5×10^7	2.5×10^4	1.7×10^3	84.3					89
(Deut)Fe[O(CH_2)3Py]	20×10^7	7×10^4	2.5×10^3	57.4					89
(T_{piv}PP)Fe(1-MeIm)	4.30×10^8	230	1.4×10^5	1.02					90

[a] EtCN solvent. [b] THF solvent. [c] This work; Abbreviations used: Piv_3(5ClmP)P = α,β,γ-tris(*o*-pivalamidophenyl)-δ-[*o*-(3-*N*-imidazolylvaleramido)phenyl]porphyrin; Piv_3(4ClmP)P = α,β,γ-tris(*o*-pivalamidophenyl)-δ-[*o*-(3-*N*-imidazolylbutyramido)]phenylporphyrin; T_{piv}PP = *meso*-α,β,γ,δ-tetrakis(*o*-pivalamidophenyl)porphyrin; MedPoc = "medium" pocket porphyrin; PocPiv = "small" pocket porphyrin; TPP = *meso*-tetraphenylporphyrin; durene-4/4 = durene-capped porphyrin; C_2-cap = 5,10,15,20-[pyromellitoyl(tetrakis(*o*-oxyethoxyphenyl))]porphyrin; C_3-cap = 5,10,15,20-[pyromellitoyl(tetrakis(*o*-oxypropoxyphenyl))]porphyrin; Deut = deuterioporphyrin; 1-MeIm = *N*-methylimidazole; 1,2-Me_2Im = 1,2-dimethylimidazole; DCIm = 1,5-dicyclohexylimidazole; Py = pyridine.

of **2** to give back **1** plus O_2). The rather high activation enthalpy ($\Delta H^{\ddagger}$ = 38.6 ± 0.2 kJ/mol) for the formation of **2** may be attributed to the need for dissociation of the strong EtCN axial ligand upon O_2-binding, with the positive entropy of activation ($\Delta S^{\ddagger}$ = 42 ± 1 J/K mol) being also consistent with the importance of axial ligand (EtCN) dissociation. Since this ligand dissociation situation is not present in the other heme systems listed in Table 5 (which employ tethered axial bases and/or superstructured O_2-binding pockets), their dioxygen-binding leads to negative activation entropies. Furthermore, the reaction enthalpy (EtCN, $\Delta H°$ = −40 ± 5 kJ/mol; THF, $\Delta H°$ = −37.5 ± 0.4 kJ/mol) and entropy (EtCN, $\Delta S°$ = −105 ± 23 J/K mol; THF, $\Delta S°$ = −109 ± 2 J/K mol) are smaller for **1** than for the majority of the other systems (Table 5), suggesting again the influence of the fluorine substituents upon dioxygen-binding: the O_2-binding (O_2^- to Fe^{III}) is weaker in (S)(F_8TPP)-Fe^{III}-(O_2^-) (**2**).

Reversible Diiron-μ-Peroxo Formation: [(F_8TPP)Fe^{III}]$_2$-(O_2^{2-}) (3). UV−Visible Spectroscopy. Addition of dioxygen to a solution of (F_8TPP)Fe^{II} (**1**) in CH_2Cl_2 or toluene at low temperature revealed the presence (by UV−visible spectroscopy) of a stable species, **3**, which eventually decomposes (thermally) to the ferric hydroxy complex, (F_8TPP)Fe^{III}-OH (**5**).

In toluene solvent, (F_8TPP)Fe^{II} (**1**) exhibits UV−visible features at 422 (Soret), 528, and 556 nm (193 K, Figure 6). Upon exposure to dioxygen, an immediate change in the spectrum is observed [λ_{max} = 418 (Soret), 536 nm]; similar behavior is also observed in CH_2Cl_2 (see below). Given the lack of a suitable axial base ligand in these noncoordinating solvents, we formulate the intermediate species formed as the dinuclear peroxo-bridged complex [(F_8TPP)Fe^{III}]$_2$-(O_2^{2-}) (**3**) (Scheme 2), even though the UV−visible spectrum contains features very similar to those of (F_8TPP)Fe^{III}-(O_2^-) (**2**). This formulation is based upon our dioxygen-uptake measurements and ^{2}H NMR spectroscopic supporting evidence, as well as (in part) the extensive work of Balch and co-workers, which established μ-peroxo diiron PFe^{III}-(O_2^{2-})-Fe^{III}P adduct formation with the TPP and TMP systems.[58−60,91]

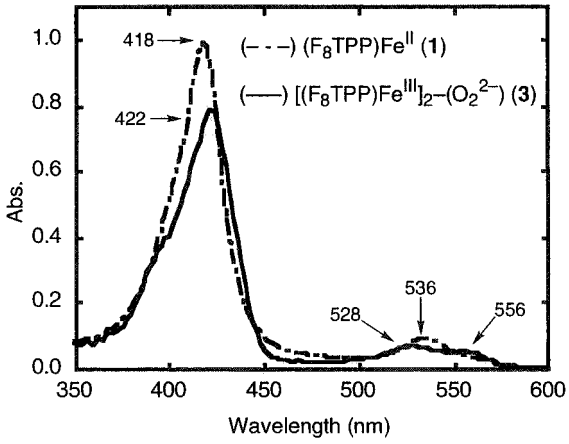

Figure 6. UV−visible spectra of the (F_8TPP)Fe^{II} (**1**)/[(F_8TPP)Fe^{III}]$_2$-(O_2^{2-}) (**3**) reversible dioxygenation reaction in toluene at 193 K.

As was the case with the mononuclear iron(III)-superoxo complex, (S)(F_8TPP)Fe^{III}-(O_2^-) (**2**), the dinuclear peroxo-bridged complex [(F_8TPP)Fe^{III}]$_2$-(O_2^{2-}) (**3**) also shows dioxygen-binding reversibility in toluene at 193 K, releasing O_2 (as detected by a qualitative alkaline pyrogallol test; see Experimental Section) and giving back the starting reduced complex

(81) Traylor, T. G.; White, D. K.; Campbell, D. H.; Berzinis, A. P. *J. Am. Chem. Soc.* **1981**, *103*, 4932−4936.
(82) Collman, J. P.; Brauman, J. I.; Iverson, B. L.; Sessler, J.; Morris, R. M.; Gibson, Q. H. *J. Am. Chem. Soc.* **1983**, *105*, 3052−3064.
(83) Wang, M. R.; Hoffman, B. M.; Shire, S. J.; Gurd, F. R. N. *J. Am. Chem. Soc.* **1979**, *101*, 7394−7398.
(84) Traylor, T. G.; Berzinis, A. P. *Proc. Natl. Acad. Sci., U.S.A.* **1980**, *77*, 3171−3175.
(85) Traylor, T. G.; Mitchell, M. J.; Tsuchiya, S.; Campbell, D. H.; Stynes, D. V.; Koga, N. *J. Am. Chem. Soc.* **1981**, *103*, 5234−5236.
(86) David, S.; James, B. R.; Dolphin, D.; Traylor, T. G.; Lopez, M. A. *J. Am. Chem. Soc.* **1994**, *116*, 6−14.
(87) Hashimoto, T.; Dyer, R. L.; Crossley, M. J.; Baldwin, J. E.; Basolo, F. *J. Am. Chem. Soc.* **1982**, *104*, 2101−2109.
(88) Rose, E. J.; Venkatasubramanian, P. N.; Swartz, J. C.; Jones, R. D.; Basolo, F.; Hoffman, B. M. *Proc. Natl. Acad. Sci., U.S.A.* **1982**, *79*, 5742−5745.
(89) Lavalette, D.; Momenteau, M. *J. Chem. Soc., Perkin Trans.* **1982**, 385−388.
(90) Lavalette, D.; Tetreau, C.; Momenteau, M.; Mispelter, J.; Lhoste, J.-M.; Wuenschell, G. E.; Reed, C. *Laser Chem.* **1990**, *10*, 297−318.
(91) Chin, D.-H.; Del Gaudio, J.; La Mar, G. N.; Balch, A. L. *J. Am. Chem. Soc.* **1977**, *99*, 5486−5488.

Scheme 2

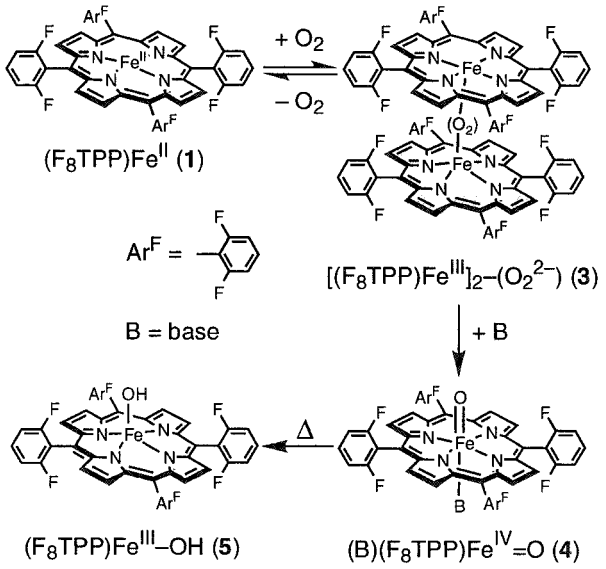

(F_8TPP)Fe^{II} (**1**). Reversibility was accomplished by application of a vacuum and subsequent bubbling of argon directly into the solution containing the heme-O_2 complex at 193 K; vacuum alone was unable to accomplish this. Slight decomposition to (F_8TPP)Fe^{III}-OH (**5**) [UV−visible: 408 (Soret) and 572 nm] was seen only after several cycles of O_2-binding and release and was most easily followed by UV−visible spectroscopic monitoring, Figure S9. This behavior contrasts with the irreversible O_2-binding observed for other PFe^{III}-(O_2^{2-})-Fe^{III}P porphyrinate−iron(III) systems as studied by Balch and coworkers.[59] We speculate that the electron-withdrawing fluorine substituents weaken the Fe−O bonds in **3** (as compared to Balch's TMP or TPP systems), shifting the equilibrium and thereby allowing for the reversibility to be easily observed under these mild conditions. Furthermore, toluene as solvent (vs CH_2Cl_2) may be critical for reversibility: the crystal structure of **1**, as the bis(toluene) solvate, shows the close contacts of toluene to the metal center, and these solvent "ligands" may promote stabilization of the (F_8TPP)Fe^{II} (**1**) complex. Complex **3** was found to be irreversible in dichloromethane, with all attempts at reversing the O_2-binding leading to formation of the decomposition complex **5**. Additionally, formation of **3** from reaction of **1** with dioxygen in noncoordinating solvents was too fast to be observed by stopped-flow spectrophotometry.

Dioxygen-Uptake Stoichiometry of (F_8TPP)Fe^{II} (1). Consistent with the formation of a μ-peroxo-bridged diiron complex was the confirmation of the dioxygen uptake of **1**, utilizing a spectrophotometric titration methodology (see Experimental Section). The UV−visible spectrum of (F_8TPP)Fe^{II} (**1**) is shown in Figure S10 [λ_{max} = 421 nm (Soret); CH_2Cl_2, 193 K]. Addition of 0.3 equiv of dioxygen (via syringe) showed a slow and partial conversion to the spectrum corresponding to [(F_8TPP)Fe^{III}]$_2$-(O_2^{2-}) (**3**) [λ_{max} = 414 (Soret), 535 nm]. An additional 0.1 equiv (0.4 equiv total) of dioxygen showed further formation of **3**, which neared completion after 0.5 equiv total dioxygen added. A final 0.05 equiv of O_2 aliquot (0.55 equiv O_2 total) showed the full formation of complex **3**, after which the injection of a large excess (>100 equiv) of dioxygen showed no further spectral changes. Thus, complete formation of [(F_8TPP)Fe^{III}]$_2$-(O_2^{2-}) (**3**) was accomplished with an overall oxygenation stoichiometry of 0.5−0.55 equiv of O_2 per equiv of (F_8TPP)-Fe^{II} (**1**), in agreement with the formulation of **3** as the heme-peroxo-heme dinuclear complex depicted in Scheme 2.

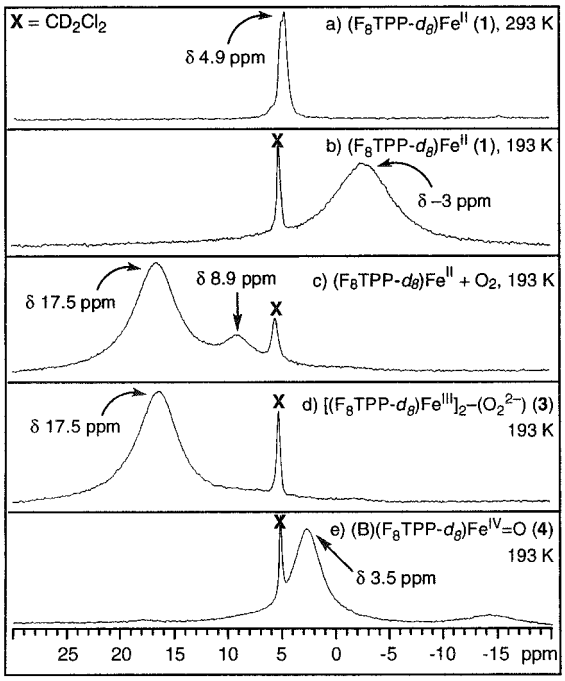

Figure 7. ^{2}H NMR of the oxygenation reaction of (F_8TPP-d_8)Fe^{II} (**1**-d_8) in CH_2Cl_2 at 193 K. Formation of the μ-peroxo dimer [(F_8TPP-d_8)Fe^{III}]$_2$-(O_2^{2-}) (**3**-d_8) and the subsequent O−O bond cleavage reaction giving (F_8TPP-d_8)Fe^{IV}=O (**4**-d_8) upon addition of DMAP (= B) are also shown. See text for further explanation.

NMR Spectroscopic Characterization of [(F_8TPP-d_8)-Fe^{III}]$_2$-(O_2^{2-}) (3-d_8). ^{2}H NMR spectroscopy was used to follow the oxygenation reaction of **1**-d_8 in CH_2Cl_2 (Figure 7). As mentioned (vide supra), the pyrrole resonance at δ 4.9 ppm (Figure 7a, 293 K) for **1**-d_8 is indicative of an intermediate spin (S = 1) system,[49,92] an observation that shows the lack of an axial base ligand for the ferrous-heme; this resonance shifts to δ −3 ppm upon cooling to 193 K (Figure 7b). Addition of dioxygen (via syringe) to the chilled (dry ice) NMR tube containing a solution of **1**-d_8 in CH_2Cl_2 gives an interesting result: two pyrrole resonances are observed (Figure 7c), with the main resonance at δ 17.5 ppm and a second minor one occurring at δ 8.9 ppm. We assign the δ 17.5 ppm feature to the dinuclear peroxo-bridged complex [(F_8TPP-d_8)Fe^{III}]$_2$-(O_2^{2-}) (**3**-d_8), which is in very good agreement with the pyrrole-H resonances of previously characterized heme-peroxo-heme complexes (Table 4).

We have also assigned the second feature at δ 8.9 ppm as a mononuclear iron(III)-superoxo complex, (F_8TPP)Fe^{III}-(O_2^-), similar to **2**, but lacking the coordinated axial (solvent) ligand. The occurrence of the (P)Fe^{III}-(O_2^-) superoxo species in noncoordinating solvents was observed earlier by Balch and coworkers for TMP (toluene solvent, −100 °C, resonance Raman spectroscopy)[58,93] and by others (see Table 4). Complete transformation to the μ-peroxo complex **3** occurs upon warming the sample to 223 K for a few minutes, with stabilization of this species accomplished by rechilling to 193 K; the spectrum of only the pure dinuclear peroxo-bridged complex [(F_8TPP-d_8)Fe^{III}]$_2$-(O_2^{2-}) (**3**-d_8) is then observed, Figure 7d. Thus, oxygenation of (F_8TPP)Fe^{II} (**1**) in CH_2Cl_2 not only gives the expected dinuclear μ-peroxo complex **3** but also shows an initial

(92) Goff, H.; La Mar, G. N.; Reed, C. A. *J. Am. Chem. Soc.* **1977**, *99*, 3641−3646.
(93) Mizutani, Y.; Hashimoto, S.; Kitagawa, T. *J. Am. Chem. Soc.* **1990**, *112*, 6809−6814.

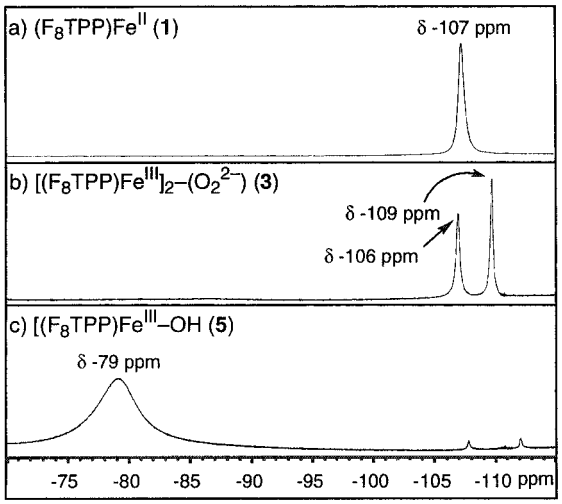

Figure 8. ^{19}F NMR spectroscopic monitoring of the oxygenation reaction of (F_8TPP)Fe^{II} (**1**) in CH_2Cl_2 at 193 K.

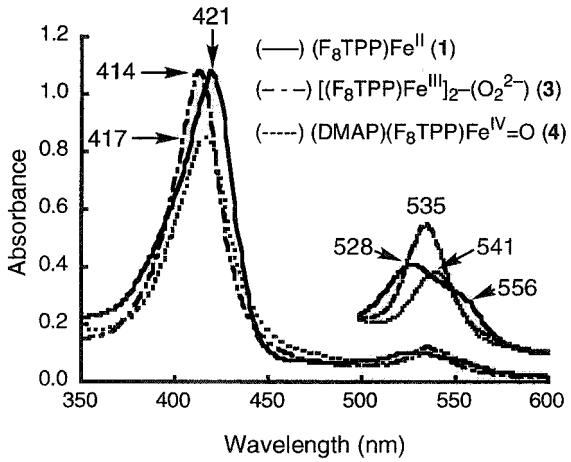

Figure 9. UV−visible spectra of (F_8TPP)Fe^{II} (**1**), [(F_8TPP)Fe^{III}]$_2$-(O_2^{2-}) (**3**), and (DMAP)(F_8TPP)Fe^{IV}=O (**4**) in CH_2Cl_2 at 193 K.

minor formation of a heme-superoxo complex, [(F_8TPP)Fe^{III}-(O_2^-)] (without axial base), which rearranges at higher temperatures to form **3**.

^{19}F NMR spectroscopy was used to further investigate this chemistry. Complex (F_8TPP)Fe^{II} (**1**) exhibits a single fluorine resonance at δ −107 ppm (CH_2Cl_2, 193 K, Figure 8a), implying an equivalent environment for all fluorine substituents. Upon oxygenation and slight warming to 233 K to form pure [(F_8TPP)Fe^{III}]$_2$-(O_2^{2-}) (**3**), two fluorine resonances were observed at δ −106 and −109 ppm, Figure 8b. The asymmetry of complex **3** can rationalize the differences in the fluorine environment of the 2,6-difluorophenyl substituents, with one resonance due to the fluorines on the "inner" peroxo side of the porphyrin macrocycle and the second resonance being attributed to those fluorines on the other "outer" side. Upon decomposition of **3**, forming (F_8TPP)Fe^{III}-OH (**5**), a single broad fluorine resonance is observed (Figure 8c) at δ −79 ppm (assignment confirmed by ^{19}F NMR spectroscopy on authentic **5**).

Iron(IV)-Oxo (Ferryl) Formation: (B)(F_8TPP)Fe^{IV}=O (4). The ^2H NMR investigations of the dinuclear peroxo-bridged complex [(F_8TPP)Fe^{III}]$_2$-(O_2^{2-}) (**3**) led us to study its chemical reactivity with respect to the addition of exogenous axial base ligands (B), such as 4-(dimethylamino)pyridine (DMAP) or tetrahydrofuran, to see if the F_8TPPH_2 ligand, with its electron-withdrawing substituents, is able to stabilize a high-valent iron(IV) oxo ferryl species. Earlier studies[58,61−63,94] established the formation of ferryl species (by NMR spectroscopy) after addition of nitrogenous bases (i.e., 1-methylimidazole) to the μ-peroxo dinuclear complexes, PFe^{III}-(O_2^{2-})-Fe^{III}P, of tetraarylporphyrin systems, and we followed the same methodology to establish this chemistry with the F_8TPPH_2 porphyrin ligand. Nam and co-workers[95] have also reported the formation of a similar five-coordinate ferryl species, (F_8TPP)Fe^{IV}=O, using 3-chloroperoxybenzoic acid, but the UV−visible characterization (Table 7) was performed in acetonitrile solvent and without the presence of an axial base ligand.

Addition of 1 equiv of DMAP (by syringe) to a chilled NMR tube containing the diiron peroxo-bridged complex [(F_8TPP-d_8)Fe^{III}]$_2$-(O_2^{2-}) (**3**-d_8) (Figure 7d, $\delta_{pyrrole}$ = 17.5 ppm) in methylene chloride at 193 K led to the immediate formation of a new species (Figure 7e, $\delta_{pyrrole}$ = 3.5 ppm). This is consistent with the literature values of the distinctive pyrrole-H resonances for the previously studied six-coordinate ferryl complexes (Table 4). We thus formulate this species as the six-coordinate high-valent iron(IV)-oxo (ferryl) complex (DMAP)(F_8TPP-d_8)-Fe^{IV}=O (**4**-d_8), Scheme 2. Species **4**-d_8 is stable indefinitely between 193 and 223 K; however, immediate formation of (F_8-TPP-d_8)Fe^{III}-OH (**5**-d_8) ($\delta_{pyrrole}$ = 125 ppm, CH_2Cl_2, 193 K) is observed upon warming.

We also investigated the ability of tetrahydrofuran, a non-nitrogen donating base, to possibly effect a similar homolytic O−O bond cleavage reaction of [(F_8TPP)Fe^{III}]$_2$-(O_2^{2-}) (**3**) to form the ferryl species **4**. Upon addition of THF (excess) to **3**-d_8 at 193 K in methylene chloride, the decomposition product **5**-d_8 was observed. Given that ferryl species are known to be stable in THF solvent (Tables 4 and 7),[96,97] we suggest that the μ-peroxo dinuclear complex [(F_8TPP)Fe^{III}]$_2$-(O_2^{2-}) (**3**) instead undergoes a direct reaction with THF to rapidly form (F_8TPP)-Fe^{III}-OH (**5**).

UV−visible spectroscopy was also utilized for further characterization of (B)(F_8TPP)Fe^{IV}=O (**4**) (B = DMAP). Oxygenation of (F_8TPP)Fe^{II} (**1**) [Figure 9: λ_{max} = 420 (Soret), 528, 558 (sh) nm; CH_2Cl_2, 193 K] reveals the formation of [(F_8-TPP)Fe^{III}]$_2$-(O_2^{2-}) (**3**) [λ_{max} = 414 (Soret) and 535 nm], comparable to the spectral features observed for toluene solvent. Addition of 1 equiv of DMAP (per Fe) gave (B)(F_8TPP)Fe^{IV}=O (**4**) (B = DMAP) with features at 417 (Soret) and 541 nm, similar to the other previously characterized Fe^{IV}=O ferryl species, Table 7.

Summary

Following closely the comprehensive studies by Balch and co-workers for other heme systems, we have utilized multinuclear NMR and UV−visible spectroscopies to determine the dioxygen reactivity of (F_8TPP)Fe^{II} (**1**) under various conditions of solvent and temperature. In coordinating solvents such as THF, propionitrile, and acetone, (F_8TPP)Fe^{II} (**1**) reacts with dioxygen at low temperature to form a stable heme-superoxo complex, (S)(F_8TPP)Fe^{III}-(O_2^-) (**2**) (S = solvent). As with other PFe^{III}-(O_2^-) complexes, we have shown **2** to be fully reversible

(94) Balch, A. L.; La Mar, G. N.; Latos-Grazynski, L.; Renner, M. W.; Thanabal, V. *J. Am. Chem. Soc.* **1985**, *107*, 3003−3007.
(95) Nam, W.; Lim, M. H.; Moon, S. K.; Kim, C. *J. Am. Chem. Soc.* **2000**, *122*, 10805−10809.
(96) Schappacher, M.; Weiss, R.; Montiel-Montoya, R.; Trautwein, A. X.; Tabard, A. *J. Am. Chem. Soc.* **1985**, *107*, 3736.
(97) Yeh, C.-Y.; Chang, C. J.; Nocera, D. G. *J. Am. Chem. Soc.* **2001**, *123*, 1513−1514.

Table 7. UV−Visible Data for PFe^{IV}═O (Ferryl) Complexes Under Various Conditions[a]

Fe^{IV}═O complex	λ_{max}	solvent	temp (K)	ref
(DMAP)(F_8TPP)Fe^{IV}═O (4)	417, 541	CH_2Cl_2	193	this work
(F_8TPP)Fe^{IV}═O	n/a, 540[b]	CH_3CN/CH_2Cl_2	233	95
(F_{20}TPP)Fe^{IV}═O	∼410,[b] 545	CH_3CN/CH_2Cl_2	233	95, 98
(THF)(Cl_8TPP)Fe^{IV}═O	417, 551	THF	223	96
(DMF)(Cl_8TPP)Fe^{IV}═O	419, 554	DMF	223	96
(1-MeIm)(Cl_8TPP)Fe^{IV}═O	421, 561	THF	223	96
(HPX)Fe^{IV}═O	418, 555	THF	212	97
(TMP)Fe^{IV}═O	∼420,[b] 545	CH_2Cl_2	233	99
(TMP)Fe^{IV}═O	418, 545	CH_2Cl_2/TBAP	233	100
(TMP)Fe^{IV}═O	418, 540	benzene	RT	101
(THF)(TpivPP)Fe^{IV}═O	419, 550	THF	203	96
(1-MeIm)(TpivPP)Fe^{IV}═O	426, 560	THF	203	96
(1-MeIm)(TPP)Fe^{IV}═O	427, 555, 563	toluene	183	102
(1-MeIm)(PPDME)Fe^{IV}═O	416, 543, 555	toluene	183	102
(1-MeIm)(OEP)Fe^{IV}═O	406, 535, 546	toluene	183	102

[a] F_{20}TPP = *meso*-tetrakis(pentaflurorphenyl)porphyrin; Cl_8TPP = *meso*-tetrakis(2,6-dichlorophenyl)porphyrin; TMP = *meso*-tetramesitylporphyrin; TPP = *meso*-tetraphenylporphyrin; TpivPP = *meso*-tetrakis(α,α,α,α-*o*-pivalamidophenyl)porphyrin; PPDME = protoporphyrin IX dimethyl ester; OEP = octaethylporphyrin; DMAP = 4-(dimethylamino)pyridine; 1-MeIm = *N*-methylimidazole. [b] Exact wavelength not given, but spectrum available.

by benchtop UV−visible spectroscopy, and stopped-flow spectrophotometry was used to determine the kinetics and thermodynamics of dioxygen-binding to **1**. Although the formation of **2** in THF solvent was within the mixing time of the apparatus, equilibrium data were obtained from temperature-dependent investigations. However, O_2-binding to **1** in EtCN was sufficiently slow as to provide kinetic insights. Confirmation of **2** as a heme-superoxo complex came from both O_2-uptake manometry and ^{2}H NMR spectroscopy. Furthermore, ^{19}F NMR spectroscopy was also employed to characterize **2** and is, to our knowledge, the first example of ^{19}F NMR used to examine these types of dioxygen adducts.

We have also examined the dioxygen reactivity of **1** in noncoordinating solvents (CH_2Cl_2, toluene) to yield the heme-peroxo-heme dimer [(F_8TPP)Fe^{III}]$_2$-(O_2^{2-}) (**3**) at low temperature. Unlike the PFe^{III}-(O_2^{2-})-Fe^{III}P peroxo-bridged systems studied by Balch using other porphyrin ligands, the formation of **3** is fully reversible in toluene solvent, probably due to the electron-withdrawing nature of the F_8TPP porphyrin. Formulation of the dioxygen adduct in noncoordinating solvents as peroxo complex **3** was confirmed by dioxygen-uptake measurements (spectrophotometric titration) and by ^{2}H NMR spectroscopy in CH_2Cl_2. Again, ^{19}F NMR spectroscopy was used to further characterize **3**. The chemical reactivity of **3** to form (B)-(F_8TPP)Fe^{IV}═O (**4**) (B = DMAP) was also explored by UV−visible and ^{2}H NMR spectroscopies, by addition of a nitrogen axial base ligand. Thus, formation of a ferryl species such as (DMAP)(F_8TPP)Fe^{IV}═O (**4**) was confirmed by these studies.

In conclusion, we have studied the dioxygen reactivity of (F_8-TPP)Fe^{II} (**1**) under various conditions and have concluded that the reaction of **1** with O_2 is similar to other heme systems such as (TPP)Fe^{II} and (TMP)Fe^{II}, with one notable exception: the formation of the heme-peroxo-heme dimer, complex **3**, is fully reversible. These studies of (F_8TPP)Fe^{II} (**1**) with dioxygen lay the groundwork for better understanding $PFe^{II}/Cu^{I}(L)/O_2$ reactions and will serve to help elucidate the rich chemistry of heme-Cu systems as models for cytochrome *c* oxidase.

Experimental Section

Materials and Methods. Reagents and solvents were purchased from commercial sources and were of reagent quality unless otherwise stated. All solvents were distilled under argon prior to use. Dichloromethane (CH_2Cl_2), acetonitrile (CH_3CN), and heptane were distilled directly from CaH_2. Propionitrile (C_2H_5CN) was first distilled over P_4O_{10}, then refluxed and distilled over CaH_2. Diethyl ether was distilled from Na/benzophenone. Preparation and handling of air-sensitive materials was carried out under an argon atmosphere using standard Schlenk techniques. Solvents and solutions were deoxygenated either by repeated freeze−pump−thaw cycles or by bubbling of argon (20−30 min) directly through the solution. Solid samples were stored and transferred, and samples for UV−visible and NMR spectroscopies were prepared, in an MBraun LabMaster 130 inert atmosphere (<1 ppm O_2, <1 ppm H_2O) glovebox under nitrogen atmosphere. Ultrahigh-purity O_2 (99.994%) was purchased from WSC, Baltimore, MD.

NMR spectra were measured on a Varian NMR instrument. All spectra were recorded in 5 mm o.d. NMR tubes, and chemical shifts were reported as δ (ppm) values downfield from an internal standard of Me_4Si (^{1}H), as δ (ppm) values calibrated to natural abundance deuterium solvent peaks with shifts referenced downfield from TMS (^{2}H), or as δ (ppm) values referenced to an external standard of α,α,α-trifluorotoluene at δ −63.73 ppm (^{19}F). Low-temperature UV−visible spectral studies were carried out with a Hewlett-Packard 8453 diode array spectrometer equipped with HPChemstation software. The spectrometer was equipped with a variable-temperature dewar and cuvette assembly as described elsewhere.[103,104] Fast atomic bombardment (FAB-MS) mass spectra were obtained with a double-focusing Vacuum Generator 70-S (VG 70-S) gas chromatography/mass spectrometer. Matrix-assisted laser desorption ionization time-of-flight (MALDI-TOF-MS) mass spectra were recorded on a Kratos Analytical Kompact MALDI 4 mass spectrometer equipped with a 337 nm nitrogen laser (20 kV extraction voltage). No matrix was necessary for the MALDI-TOF-MS given that the porphyrin ligand was sufficient for laser desorption.

F_8TPPH$_2$. Tetrakis(2,6-difluorophenyl)porphyrin was prepared by standard benzaldehyde-pyrrole condensation in propionic acid/nitrobenzene reflux, in a procedure modified from that previously[65,105,106] reported: To a 2000 mL two-neck round-bottom flask equipped with reflux condensor was added 1000 mL of propionic acid, 250 mL of

(98) Nam, W.; Lim, M. H.; Oh, S.-Y.; Lee, J. H.; Lee, H. J.; Woo, S. K.; Kim, C.; Shin, W. *Angew. Chem., Int. Ed.* **2000**, *39*, 3646−3649.
(99) Nam, W.; Lim, M. H.; Oh, S.-Y. *Inorg. Chem.* **2000**, *39*, 5572−5575.
(100) Groves, J. T.; Gilbert, J. A. *Inorg. Chem.* **1986**, *25*, 123.
(101) Groves, J. T.; Gross, Z.; Stern, M. K. *Inorg. Chem.* **1994**, *33*, 5065−5072.
(102) Oertling, W. A.; Kean, R. T.; Wever, R.; Babcock, G. T. *Inorg. Chem.* **1991**, *29*, 2633−2645.
(103) Karlin, K. D.; Cruse, R. W.; Gultneh, Y.; Farooq, A.; Hayes, J. C.; Zubieta, J. *J. Am. Chem. Soc.* **1987**, *109*, 2668−2679.
(104) Karlin, K. D.; Haka, M. S.; Cruse, R. W.; Meyer, G. J.; Farooq, A.; Gultneh, Y.; Hayes, J. C.; Zubieta, J. *J. Am. Chem. Soc.* **1988**, *110*, 1196−1207.
(105) Fuhrhop, J.-H.; Smith, K. M. In *Porphyrins and Metalloporphyrins*; Smith, K. M., Ed.; Elsevier: New York, 1975; pp 769−770.
(106) Adler, A. D.; Longo, F. R.; Finarelli, J.; Goldmacher, J.; Assour, J.; Korsakoff, L. *J. Org. Chem.* **1967**, *32*, 476.

nitrobenzene, and 25.0 g (176 mmol) of 2,6-difluorobenzaldehyde. The solution was brought to reflux, after which 12.0 g (179 mmol) of pyrrole was added dropwise to the reaction flask, causing an immediately darkening of the yellow solution to black. After 2 h, the reaction mixture was cooled to room temperature and placed in a freezer (−20 °C) for several days. The resulting purple solid was collected via filtration over Celite, washed with water (2000 mL), dried over air, and removed from Celite with CH_2Cl_2 (2000 mL). The solution was dried over $MgSO_4$, filtered, and concentrated to dryness via rotary evaporation. The crude material was first purified over an alumina column (35 cm × 5.5 cm o.d.) using methylene chloride ($R_f = 0.99$) eluent and then purified further over a silica column (30 cm × 5.5 cm o.d.) with 50:50 CH_2Cl_2/hexanes ($R_f = 0.57$). Solvent was removed via rotary evaporation, and the solid obtained was dried in vacuo for 2 h. F_8TPPH_2 was isolated as a free flowing purple solid in 6.4% yield (8.5 g). UV−vis (CH_2Cl_2): 412 (Soret), 507, 584 nm. ^{1}H NMR ($CDCl_3$): δ 8.86 (s, 8 H, pyrrole-H), 7.79 (m, 4 H, *p*-phenyl-H), 7.38 (t, $J = 8.39$ Hz, 8 H, *m*-phenyl-H), −2.75 (s, 2 H, NH); ^{19}F NMR ($CDCl_3$): δ −109.17 (t, $J_{HF} = 6.0$ Hz, *o*-phenyl-F). MALDI-TOF-MS (*m*/*z*): 759.6 $(M + H^+)^+$.

F_8TPPH_2-*d*$_8$. In a procedure modified from that previously reported,[66] the pyrrole-deuterated F_8TPPH_2-d_8 was prepared in a one-pot reaction in which the pyrrole proton−deuteron exchange was effected prior to condensation: To a 2000 mL two-neck round-bottom flask was added under argon 1 L of propionic anhydride (97%) and 175 mL of D_2O (99.9 atom % D), and the solution was brought to reflux for 1 h. To this deuterated propionic acid was added under argon 12.0 g (179 mmol) of pyrrole, and the reaction mixture was refluxed for an additional hour. In air, 250 mL of nitrobenzene and 25.0 g (176 mmol) of 2,6-difluorobenzaldehyde were added. Reflux continued for an hour, after which the reaction mixture was cooled to room temperature and placed in a freezer (−20 °C) for several days. The resulting purple solid was collected and purified as above for F_8TPPH_2. F_8TPPH_2-d_8 was isolated as a free flowing purple solid in 6.5% yield (8.5 g). UV−visible and ^{1}H and ^{19}F NMR spectroscopic characterization were the same as for F_8TPPH_2. ^{2}H NMR ($CHCl_3$): δ 8.94 (s, pyrrole-D). FAB-MS (*m*/*z*): 766 $(M + H^+)^+$. Mass spectroscopic analysis reveals that F_8TPPH_2-d_8 made by this procedure is minimally 90 atom % deuterated for the pyrrole hydrogens.

$(F_8TPP)Fe^{III}Cl$. To a refluxing solution of F_8TPPH_2 (1.0 g, 1.32 mmol) in deoxygenated DMF (250 mL) under Ar atmosphere was added anhydrous $FeCl_2$ (3.5 g, 27.6 mmol) in approximate 20-fold molar excess. After continued stirring and reflux for 1 h, the reaction mixture was cooled and exposed to air, and addition of 1 L of 2 M HCl(aq) caused a solid purple precipitate to form. The solid material was collected by filtration using a medium-porosity filter frit and dissolved in 500 mL of CH_2Cl_2 to give a dark red solution. This organic solution was washed with 1 M HCl (2 × 500 mL) and water (1 × 500 mL), dried over Na_2SO_4, and filtered, and the crude material (filtrate) was adsorbed onto silica. Purification over a silica column (35 cm × 4.0 cm o.d.) was accomplished by removing impurities (including unmetalated ligand) with CH_2Cl_2, followed by elution of the desired product with 3% MeOH in CH_2Cl_2 ($R_f = 0.45$−0.55). Solvent was removed via rotary evaporation, and the resulting purple-black solid was precipitated from CH_2Cl_2 (50 mL) solution upon addition of heptane (450 mL). $(F_8TPP)Fe^{III}Cl$ was isolated (1.03 g, 1.22 mmol) as a black solid in 92% yield. UV−vis (CH_2Cl_2): 411, 503, 639, 772. ^{1}H NMR ($CDCl_3$): δ 81.54 (s, br, 8 H, pyrrole-H), 13.86 (s, 4 H, *m*-phenyl-H), 12.52 (s, 4 H, *m*-phenyl-H), 7.6 (s, 4 H, *p*-phenyl-H). ^{19}F NMR ($CDCl_3$): δ −76.53 (s, br, *o*-phenyl-F), −80.28 (s, br). FAB-MS (*m*/*z*): 812 $(M - Cl^-)^+$. Anal. Calcd for $C_{44}H_{20}ClF_8FeN_4$: C, 62.32; H, 2.38; N, 6.61; Found: C, 62.62; H, 2.44; N, 6.37.

$(F_8TPP$-*d*$_8)Fe^{III}Cl$. The procedure used is identical to that described above for $(F_8TPP)Fe^{III}Cl$, but utilized F_8TPPH_2-d_8 in place of F_8TPPH_2. ^{2}H NMR ($CHCl_3$): δ 80.6 (s, br, pyrrole-D). FAB-MS (*m*/*z*): 819 $(M - Cl^-)^+$.

$(F_8TPP)Fe^{II}$ (1). Under Ar, to a solution of $(F_8TPP)Fe^{III}Cl$ (1.0 g, 1.18 mmol) in deoxygenated methylene chloride (50 mL) was added 40 mL of 1 M sodium hydrosulfite in deoxygenated water. The two solutions were agitated with Ar bubbling for 30 min to ensure complete mixing, during which time the color of the organic later changed from dark red-brown to bright red. The reaction mixture was allowed to sit for ample time (∼5 min) to allow for the separation of the two layers, after which the organic layer was allowed to slowly pass through a Schlenk filter tube (coarse porosity) over which was packed a small plug of anhydrous sodium sulfate (∼4 g). The solvent was concentrated in vacuo, and addition of deoxygenated heptane precipitated **1** as a opaque crystalline solid (875 mg, 1.08 mmol) in 91% yield. UV−vis: THF, 421, 542; propionitrile, 414, 424, 528; toluene, 422, 528, 558 (sh); CH_2Cl_2, 422, 528, 558 (sh). ^{1}H NMR (THF-d_8): δ 56 (s, pyrrole-H, 8 H), 8.38 (s, *p*-phenyl-H, 4H), 7.15 (s, *m*-phenyl-H, 8H). ^{19}F NMR (THF-d_8): δ −111.5 (*o*-phenyl-F). MALDI-TOF-MS (*m*/*z*): 813 $(M + H^+)^+$.

$(F_8TPP$-*d*$_8)Fe^{II}$ (1-*d*$_8$). The procedure used is identical to that described above for $(F_8TPP)Fe^{II}$ (**1**), except $(F_8TPP$-$d_8)Fe^{III}Cl$ was used instead of $(F_8TPP)Fe^{III}Cl$. ^{2}H NMR (THF): δ 56 (s, br, pyrrole-D). MALDI-TOF-MS (*m*/*z*): 820 $(M + H^+)^+$.

Crystallographic Structural Determination of $(F_8TPP)Fe^{II}\cdot(C_7H_8)_2$ (1·$(C_7H_8)_2$). Recrystallization of **1** from toluene/heptane under argon atmosphere gave large purple-red crystals suitable for X-ray diffraction. Crystal data collection and refinement parameters are given in Table 1. The systematic absences in the diffraction data are consistent for the *C*-centered monoclinic space groups, *Cc* and C2/*c*. The *E*-statistics and the value of *Z* suggested the centrosymmetric space group, which yielded chemically reasonable and computationally stable results of refinement. The structure was solved using direct methods, completed by subsequent difference Fourier syntheses, and refined by full-matrix least-squares procedures. The asymmetric unit consists of half of **1** located on an inversion center and a molecule of toluene. All non-hydrogen atoms were refined with anisotropic displacement coefficients, and the hydrogen atoms were treated as idealized contributions.

All software and sources of the scattering factors are contained in the SHELXTL (5.1) program library (G. Sheldrick, Siemens XRD, Madison, WI). The X-ray table for **1**·$(C_7H_8)_2$ is found in the text (Table 1), while the full X-ray reports for both **1**·$(C_7H_8)_2$ and $(F_8TPP)Fe^{III}$-Cl can be found in the Supporting Information.

Dioxygen-Uptake Manometry of $F_8TPP)Fe^{II}$ (1) in THF Solvent. O_2 absorption by **1** at 193 K was monitored at constant pressure in a glass buret as previously described.[103,104] A sidearm Schlenk flask containing 10 mL of deoxygenated THF solution of $(F_8TPP)Fe^{II}$ (**1**) (500 mg, 615 μmol) was attached to the manometer system and cooled to 193 K. After evacuation and degassing of the solution with repeated freeze−pump−thaw cycles, the stopcock leading to the reaction flask was closed and the buret assembly was equilibrated to 1 atm of O_2. The Schlenk flask was then opened to the manometer assembly, allowing reaction of **1** with O_2. The volume of O_2 taken up was 15.1 mL at 960 mTorr (after accounting for 4.0 mL of solvent O_2 uptake), corresponding to an Fe:O_2 ratio of 1:0.98; a second experiment at 980 mTorr required 15.6 mL, for an Fe/O_2 ratio of 1:1.03.

Dioxygen Uptake (Spectrophotometric Titration) of $F_8TPP)Fe^{II}$ (1) in CH_2Cl_2 Solvent. To an air-free cuvette assembly with sidearm stopcock and female 14/20 joint was added in a glovebox a known quantity of **1** (typically 1 mg) via stock solution (1 mg **1**/g solvent) in CH_2Cl_2. A 14/20 septum adapter (Chemglass) was used to seal the cuvette from the atmosphere, followed by two additional septa (each successively larger than the previous) wired to the septum adapter (for a total of three septa). The cuvette assmbly was then removed from the glovebox, placed into the modified low-temperature UV−visible spectrophotometer, and cooled to −80 °C. A commercially available (Potomac Airgas, Baltimore, MD) 1.01 ± 0.02 mol % O_2 in Ar gas mixture was then slowly bubbled through a two-sidearmed Schlenk flask equipped with rubber septum and oil bubbler, which allowed for continuous flow of the 1% O_2 gas mixture at atmospheric pressure. Hamilton gastight syringes (250, 500, and 1000 μL) equipped with three-way valves (for Ar purging of the syringe barrel and needle) were used to transfer exact molar quanitites of dioxygen to the cooled cuvette assembly. Typical transfer ratios included 0.3 equiv of (875 μL) dioxygen (per **1**), followed by 2 × 0.1 equiv (2 × 300 μL) and 0.05 equiv (150 μL) additions. Each addition of dioxygen directly into the solution through the multiple septa was accompanied by gentle shaking of the cuvette assembly and UV−visible spectroscopic monitoring. When no further spectral changes were detected after each successive

addition of dioxygen, the next partial equivalent was added. In this manner, it was established that full formation of the oxygen intermediate of **1** occurred between 0.5 equiv (1500 μL 1.01% O_2 in argon) and 0.55 equiv (1650 μL 1.01% O_2 in argon) of dioxygen. No spectral changes were observed from direct injection of dioxygen (>100 equiv) after the total 0.55 equiv was added. Furthermore, a second cuvette filled with the same stock solution of **1** used for the titration was directly injected with a large excess of dioxygen, and the spectrum obtained for this was nearly superimposable (with respect to λ_{max} and absorbance) to that obtained from the spectrophotometric titration. Finally, a control experiment was performed in which **1** was injected a total of five times with 500 μL of dioxygen-free argon in a manner identical to that above, with no detectable changes in the spectrum of **1** observed.

Variable-Temperature NMR Studies. Both deuterated and undeuterated solvents were distilled and degassed prior to use. In the glovebox, typically a solution containing 10−20 mg of **1** in 1 mL of solvent (deuterated solvent for ^{1}H and ^{19}F spectra, undeuterated solvent for ^{2}H) was prepared and transferred to 5 mm o.d. 8 in. Wilmad screw-cap sample tubes (528-TR-8). ^{1}H, ^{2}H, and/or ^{19}F NMR spectra were recorded at room temperature before cooling to the desired temperature. Addition of dioxygen at low temperature was carried out in the following manner: the NMR tube was removed from the spectrometer and placed either ina dry ice/acetone bath or directly into dry ice, and using a Hamilton gastight syringe, excess O_2 (99.994%; WSC, Baltimore) was bubbled directly through the solution using a long syringe needle. Addition of solutions (i.e., 4-(dimethylamino)pyridine) was also performed in a similar manner. Typical spectra were recorded at 100 kHz spectral width with no delay between 90° pulses of 7.2, 17.5, and 5.0 μs for ^{1}H (400 MHz), ^{2}H (61 MHz), and ^{19}F (376 MHz) spectra, respectively. Referencing/calibration of the spectra was performed as described above for each given temperature, and shift values are reported at the stated temperature; for ^{1}H and ^{2}H NMR spectroscopy, those resonances positive to TMS are downfield and those negative are upfield.

Evans Method Magnetic Moment Measurements. All Evans method[107,108] magnetic moment measurements were carried out in 5 mm o.d. 8 in. Wilmad screw-cap sample tubes (528-TR-8) equipped with pierceable Teflon-faced rubber septa. Coaxial insert reference capillaries were also purchased from Wilmad (WGS-5BL). In a typical experiment, the sample tube and the coaxial insert were brought into a glovebox, and a sample of **1** with known concentration and volume in deoxygenated solvent was placed in the sample tube. The coaxial insert was filled with deoxygenated solvent as well and then placed inside the sample tube, which was then sealed with the septum cap. After removal from the glovebox, ^{1}H and ^{2}H NMR spectra were obtained and referenced as normal, with the paramagnetically shifted solvent peak occurring downfield of the reference solvent peak. ^{2}H NMR was used to confirm the Evans method magnetic moment measurements since only two resonances, one corresponding to the paramagnetically shifted deuterated solvent and the second corresponding to the reference capillary deuterated solvent, were observed, thereby eliminating erroneous peak assignments or unobserveable peaks due to spectral overlap. The equation $\mu_B = 2.84\sqrt{\chi_M T/n}$ was used to calculate the magnetic moment, where T is the temperature (K) of the measurement, n is the nuclearity of the complex ($n = 1$ for **1**), and $\chi_M = -(3/4\pi)(\Delta\nu/\nu)(1000/c) + \chi_M^{sol} - \chi_D$, where χ_M^{sol} is the solvent susceptibility ($= \chi_g$, gram susceptibility of solvent, × MW of the metal complex), χ_D is the total diamagnetic correction (calculated from Pascal's constants),[109] $\Delta\nu$ is the paramagnetic shift of the solvent ($= \nu_{reference}^{solvent} - \nu_{sample}^{solvent}$, a negative value) in Hz, ν is the frequency of the NMR instrument in Hz, and c is the concentration of the metal complex (corrected for temperature by use of the temperature dependence of the solvent density). All reported magnetic moments are the average of three runs (unless otherwise stated).

Reversible O_2-Binding. In the glovebox, a solution of **1** in the desired solvent was prepared and transferred to a modified low-temperature cuvette assembly equipped with a Schlenk-type sidearm. After cooling to 193 K, generation of the dioxygen adducts was carried out by bubbling the chilled solution with dioxygen (ultrahigh purity). Removal of excess dioxygen was performed by simple application of vacuum at 193 K. Reversible binding was carried out either by bubbling the solution with argon using a syringe needle at 193 K for 15−25 min or by warming the solution to room temperature and subsequent vacuum to remove O_2 liberated during the warming process.

Alkaline Pyrogallol Test for Dioxygen Evolution. In the glovebox, a solution of **1** (40 mg) in the desired solvent (∼15 mL) was prepared and transferred to a Schlenk flask capped with a rubber septum. Bubbling of dioxygen via syringe needle at 193 K afforded the desired dioxygen adduct, either (THF)(F_8TPP)Fe^{III}-(O_2^-) (**2**) (THF solvent) or [(F_8TPP)Fe^{III}]$_2$-(O_2^{2-}) (**3**) (toluene solvent). Removal of excess O_2 was performed with multiple freeze−pump−thaw cycles (thawing temperature was 193 K), yielding a solution whose only source of dioxygen was the heme-O_2 adduct.

To a special Schlenk flask modified with a quartz cuvette and equipped with a stir bar was added 4.0 g of pyrogallol and 25 mL of deoxygenated 50% KOH(aq) solution under Ar. The alkaline pyrogallol solution was a faint beige color, and its UV−visible spectrum was recorded ($\lambda_{400\ nm} = \sim 0.035-0.04$). Using a syringe needle, argon was bubbled directly through the heme-O_2 solution at 193 K, liberating O_2 into the headspace of the Schlenk flask, which was then passed through a cannula and bubbled directly into the stirring alkaline pyrogallol solution, whose color began to darken after 1 min. After approximately 20 min, the pyrogallol solution ceased becoming darker, and its spectrum was re-recorded ($\lambda_{400\ nm} = \sim 0.4-0.45$). This process was repeated under identical conditions but without **1** present as a control and showed no significant increase in absorbance ($\lambda_{400\ nm} = \sim 0.05-0.06$).

Stopped-Flow Spectrophotometry. Rapid kinetics were followed using an SF-21 variable-temperature stopped-flow unit (Hi-Tech Scientific) combined with a TIDAS-16 HQ/UV−vis 512-16B diode array spectrometer (J & M; 507 diodes, 300−720 nm, 1.3 ms minimum sampling time). Data acquisition (up to 256 complete spectra; up to four different time bases) was performed by using the Kinspec program (J & M). For numerical analysis, all data were pretreated by factor analysis. The solvents were treated prior to use to remove impurities and water. Propionitrile was dried with phosphorus pentoxide (P_2O_5), distilled under normal pressure, and kept dry by storing over calcium hydride (CaH_2, Merck). Tetrahydrofuran was dried over sodium (using benzophenone as an indicator for the absence of water) and freshly distilled prior to use.

For (F_8TPP)Fe^{II} (**1**) in propionitrile, three series of experiments were performed with 0.249, 0.109, and 0.052 mM complex concentration (room temperature), respectively. Data for a total of 251 individual runs between 178 and 293 K with data collection times between 0.1 and 641 s were obtained. Of these, 119 data sets (over a temperature range of 178−205 K, where the formation of the Fe-superoxo species could be observed) were used for the analysis. The concentration profile based on the kinetic model **1** + $O_2 \equiv$ **2** was calculated by numerical integration using the Glofit[110] program. Thermal expansion of propionitrile was taken into account using ρ(g/mL) = (+1.0688−9.80) × 10^{-4} T (K) for the solvent density as a function of temperature. The initial O_2-concentration in propionitrile was 4.4 mM (room temperature).[111]

In tetrahydrofuran, (F_8-TPP)Fe^{II} (**1**) was studied by using three series (0.346, 0.230, and 0.090 mM). Data for a total of 189 individual runs between 182 and 303 K with data collection times between 0.1 and 651 s were obtained. Of these, 80 data sets (over a temperature range of 228−288 K) were used for the analysis of the fast initial equilibrium. The concentrations required for the calculation of the equilibrium constant by the law of mass action were received by Lambert and Beer's law (linear regression) using a fixed set of species spectra and absorbances measured at the first reaction time. Thermal expansion of

(107) Evans, D. F. *J. Chem. Soc.* **1959**, 2003.
(108) Live, D. H.; Chan, S. I. *Anal. Chem.* **1970**, *42*, 791−792.
(109) *CRC Handbook of Chemistry and Physics*, 74th ed.; Lide, D. R., Ed.; CRC Press: Boca Raton, 1993.
(110) Kinfit clone (see ref 111) converted into Matlab's computer language. Neuhold, Y.-M. Ph.D. Thesis, University of Basel, Switzerland, 1999.
(111) Karlin, K. D.; Wei, N.; Jung, B.; Kaderli, S.; Niklaus, P.; Zuberbühler, A. D. *J. Am. Chem. Soc.* **1993**, *115*, 9506−9514.

tetrahydrofuran was taken into account using ρ(g/mL) = (+1.1850−1.028) × 10^{-3} T (K) for the solvent density as a function of temperature determined by linear regression of the density data.[112] The initial O_2-concentration in tetrahydrofuran was 3.3 mM (room temperature).[113]

Acknowledgment. We are grateful to the National Institutes of Health (K.D.K., GM28962 and GM60353) and the Swiss National Science Foundation (A.D.Z.) for support of this research. R.M.K. also acknowledges support from the Howard Hughes Undergraduate Summer Research Program (Johns Hopkins University). We would also like to thank Prof. R. J. Cotter and Dr. A. S. Woods (Johns Hopkins School of Medicine) for their help in obtaining the MALDI-TOF-MS data.

(112) Carvajal, C.; Tölle, K. J.; Smid, J.; Szwarc, M. *J. Am. Chem. Soc.* **1965**, *87*, 5548−5553.

(113) The solubility of dioxygen in tetrahydrofuran was determined in the same way as in propionitrile by using an oxygen-sensitive Clark electrode. For more details see ref 111.

Supporting Information Available: Discussion of the reversible superoxo formation of (S)$(F_8TPP)Fe^{III}$-(O_2^-) (**2**) in THF and EtCN solvents (Figures S1, S2). Discussion of the dioxygen reactivity of $(F_8TPP)Fe^{II}$ in acetone solvent at 193 K (Figures S3−S5). Eyring plot for the $(F_8TPP)Fe^{II}$ (**1**) oxygenation reaction in EtCN (Figure S6). UV−visible spectra of the $(F_8TPP)Fe^{II}$ (**1**) + O_2 reaction as a function of temperature in THF solvent (Figure S7). Van't Hoff plot for the $(F_8TPP)Fe^{II}$ (**1**) oxygenation reaction in THF (Figure S8). UV−visible spectra of the $(F_8TPP)Fe^{II}$ (**1**)/$[(F_8TPP)Fe^{III}]_2$-(O_2^{2-}) (**3**) reversible oxygenation (cycling) reaction in toluene at 193 K (Figure S9). Dioxygen uptake (spectrophotometric titration) of $(F_8TPP)Fe^{II}$ (**1**) with dioxygen in CH_2Cl_2 (Figure S10). ORTEP representation of $(F_8TPP)Fe^{III}$-Cl (Figure S11). Crystal data and structure refinement, atomic coordinates, bond lengths and bond angles, anisotropic displacement coefficients, and H-atom coordinates for $(F_8TPP)Fe^{II}\cdot(C_7H_8)_2$ (**1**·$(C_7H_8)_2$) (Tables S1−S5) and $(F_8TPP)Fe^{III}$-Cl (Tables S6−S10). This material is available free of charge via the Internet at http://pubs.acs.org.

IC0105866